ANALYSIS OF THE GEOTHERMAL POTENTIAL OF THE NORTH WEST OLKARIA PROSPECT (OSERIAN SANCTUARY) IN KENYA, USING TRANSIENT ELECTROMAGNETIC METHOD AND MAGNETOTELLURIC METHOD

SIRMA CHEBET RUTH

A Thesis submitted to the Graduate School in partial fulfilment for the requirements of the of Master of Science Degree in Physics of Egerton University

EGERTON UNIVERSITY
OCTOBER 2019

DECLARATION AND RECOMMENDATION

Declaration

This thesis is my original work and has not been submitted in part or whole for an award in any institution.

Signature……... Date…….

Sirma Chebet Ruth

SM13/23514/14

Recommendation

This Thesis has been submitted with our approval as supervisors for examination according to Egerton University regulations.

Signature……..... Date…….

Dr. M.S.K. Kirui

Department of Physics

Egerton University

Signature…… Date…….

Prof. Nicholas Mariita

Geothermal Training and Research Institute

Dedan Kimathi University of Technology

COPYRIGHT

DEDICATION

I dedicate this work to my parents Mr. Nicholas Sirma and Emily Sirma. To my brothers and sister Grace, Samson, Daniel, Silas and Paul, my beloved daughter Victoria, my friends, Geophysics department of KenGen and Physics Department of Egerton University.

ACKNOWLEDGEMENT

Above all, thanks to the Almighty God, who has made all things possible. I thank Egerton University for according the opportunity to pursue Master of science degree in Physics. I would like to express my sincere appreciation to my supervisors Dr. M.S.K Kirui (Egerton University) and Prof. Nicholas Mariita (Dedan Kimathi University of Technology). The advice, mentorship, goodwill and the long discussions made gave great contribution to the production of this thesis. I acknowledge the Physics Department of Egerton University together with the members of staff for their relevant academic advice, useful insights and suggestions during the entire period of my research. Am also grateful to all the Egerton university Masters and PhD students (Physics) for their un-measurable friendship and various discussions during my stay in Egerton. I would like to express my sincere appreciation to the Geophysics department of The Kenya Electricity Generating Company (KenGen), for their indispensable support; technical guidance, advice and helpful comments from the beginning to the end of this research. Many thanks also to Elvis Oduong, Ammon Omiti and Martin Owiso (KenGen) for their assistance, knowledge and constructive discussions during processing of the data. I also want to thank the management of KenGen for allowing me to use the resistivity data that I collected in their area of license. I am also deeply indebted to the entire staff of KenGen for their hospitable support in all aspects of this work. Special thanks goes to my parents Nicholas and Emily Sirma for sponsoring my Master's studies at Egerton University, my beloved daughter Victoria, brothers, sisters and friends for being with me all along my steps of life. May the almighty God bless you all and everyone who contributed in one way or the other toward this important achievement.

ABSTRACT

The Northwest Olkaria prospect, *Oserian Sanctuary*, is part of the Greater Olkaria Geothermal Area located within the Kenyan rift valley in Nakuru County. It is bounded by the longitudes 36^0 15′E and 36^0 12′E with an estimated area of 30 km^2. Studies previously done did not adequately cover the area to the North West hence no geophysical data is available on the resistivity of key concealed geothermal structural features like thin massive heat sources and shallow faults based on subsurface resistivity distribution as most methods were largely DC. This study aimed at using the Magnetotelluric method and the Transient Electromagnetic Method to determine the electrical resistivity distribution of the subsurface and locate possible structural features controlling geothermal distribution in the prospect area by developing a 1D joint inversion of Magnetotelluric and Transient Electromagnetic data of the Olkaria North West prospect, 1D Iso-resistivity maps of the Olkaria Northwest prospect and a 1D Magnetotelluric model of the Olkaria Northwest prospect. A total of 50 Magnetotelluric soundings were analysed in this research as well as 47 corresponding central loop Transient Electromagnetic soundings. To allow the static shift correction in the 1D inversion, the Magnetotelluric data were jointly inverted with Transient Electromagnetic data. The results and interpretations of the Joint 1D inversion of Magnetotelluric and central loop Transient Electromagnetic data of Olkaria Northwest field were presented inform of resistivity Iso-maps and cross sections. Results of the interpretation show four main resistivity zones below the prospect area: a shallow superficially high resistivity zone (> 30Ωm) interpreted as unaltered rock formations and a thick pyroclastic cover, a thick dome shaped conductive layer (< 6Ωm) that extends to about 1900 m.a.s.l dominated by low temperature alteration minerals such as smectite and zeolite interpreted as the clay cap, a resistive layer (>15-50) Ωm associated with the high temperature secondary minerals such as epidote, chlorite and biotite present in the reservoir and another low conductivity layer extending to about 6,000 m.b.s.l. which is interpreted as a heat source of the Olkaria geothermal system. The study revealed that the main reservoir exists to the western side and it appears to be deeper than that in the eastern field. The conclusion characterised the Northwest Olkaria prospect as a geothermal potential having a heat source, a reservoir and a recharge system which are the main features of a geothermal system. The main reservoir to the western side appeared to be deeper than the eastern field, therefore it is recommended that the outlet wells should be to the west and the reinjection wells to the east of the prospect. Resistivity results from North West also indicated a resource boundary to the west at 1000m.a.s.l.

TABLE OF CONTENTS

LIST OF FIGURES

LIST OF ABBREVIATIONS AND ACRONYMS

AC	Alternating current
DC	Direct current
EDI	Electronic Data Interchange
EM	Electromagnetic
E	Electric field
GARS	Great Africa Rift System
GDP	Geophysical data processor
GTP	Geothermal Training Programme
GOGA	Greater Olkaria Geothermal Area
GPS	Geographical positioning System
IPP	Independent power producers
KRISP	Kenya Rift International Seismic Project
MT	Magnetotelluric
MTU	Magnetotelluric unit
m.a.s.l.	meters above sea level
m.b.s.l.	meters below sea level
S	Shift parameter
TEM	Transient electromagnetic
TDEM	Time-Domain Electromagnetic
TOFF	Turn off time
UTM	Universal Transverse Mercator coordinates system
UNU	United Nations University
USSR	Union of Soviets Socialists Republics
VR	Voltage regulator
WGS	World Geodetic System
1D	1 dimensional
2D	2 dimensional
3D	3 dimensional
XY	electric field parallel to the north
YX	electric field parallel to the east

LIST OF SYMBOLS

B	Magnetic induction
D	Electric Displacement
E	Electric field intensity
F	Frequency
I	Electrical current
H	Magnetic field intensity
J	Current density
k	Wave number
t	Time
V	Electrical potential
X	Accuracy parameter for inversion model
x, y	Initial Frame of Reference
x´, y´	Final Frame of Reference
$\hat{\mathbf{Z}}$	Impedance tensor
ε_0	Permittivity of free space
Ωm	Ohm meter
ω	Angular frequency
η	Electric Charge Density of free charges
σ	Electric Conductivity
δ	Electromagnetic Skin Depth
ρ	Apparent resistivity
Φ	Impedance phase

CHAPTER ONE
INTRODUCTION

1.1 Background information

The Government of Kenya identified geothermal energy as the solution to the common power crisis observed in the country for the better part of the last decade (Kiva, 2009). Frequent droughts and rising costs of petroleum products forced the government to review its policy on energy (Omenda and Simiyu, 2015). Moreover, the destruction of forests and other catchment areas have already demonstrated their effects on the climate and hence reliance on hydroelectricity alone is no longer an option. There is therefore a need to develop clean and environmentally friendly alternative sources of energy. The Government of Kenya in 2009 constituted a task force on accelerated development of green energy with a target of developing an extra 5000MW of electricity from renewable resources, most of which will come from geothermal sources by 2023 (Kenya Gazette, 2009).

The known geothermal prospects occur within the Kenyan rift valley where widespread volcanic activity and geothermal manifestations signify the existence of viable geothermal prospects (Omenda 2000; Ouma, 2010). Geothermal energy is a clean and renewable source for production of electricity, which is not affected by short-term fluctuations in the weather or world producer prices of oil. Once installed, maintenance costs are low and availability high as evident from the records for the Olkaria power stations in Kenya (Lagat *et al.*, 2007; Kanda *et al.*, 2011; Girdler, 2013; Omenda and Simiyu, 2015).

The transient electromagnetic method (TEM) and Magnetotelluric (MT) are geophysical methods for exploring the sub-surface resistivity structure of the earth. The two primary physical relationships which are utilized are Ampere's law and Faraday's law of induction. The three main resistivity methods which have been in use in Kenya are the Schlumberger, the Magnetotelluric method and the Transient Electromagnetic method (Girdler, 2013; Mulwa and Mariita, 2013, 2015; Wamalwa *et al*., 2013; Wamalwa and Serpa, 2013; Abdelfettah *et al*., 2016). The latter two, MT and TEM, are often used in conjunction since the two methods complement each other. These different resistivity techniques can be classed into two main groups: Direct current methods (DC) and electromagnetic (EM) methods. The common theme in each method is that, some form of current is flowing in the ground, either actively injected or current which is already there (active and passive methods, respectively). The current flow in the ground is then affected by the ground's resistivity structure which can be monitored at the surface.

Geophysical methods have a significant role in the investigation of geothermal prospects because they provide the means of finding deep sub-surface structures without drilling (Telford *et al.*, 1990; Parasnis, 1997). The choice of a particular method to apply depends on the objective, the type of the geothermal prospect and the cost of the survey. The geophysical techniques that have been previously used in geothermal energy exploration in Kenya's rift valley include direct current (DC) resistivity, gravity, transient electro-magnetic and Magnetotelluric (Girdler, 2013; Mulwa and Mariita, 2013, 2015).

1.2 Statement of the problem

Previous geophysical studies at Olkaria did not cover the area within the North West field. The major reasons were that the area had a difficult terrain which made the area difficult to survey with the presence of endangered wildlife species (rhinos) and private investors (Oserian development company and lapeive limited). The resistivity structure of the area was unknown as access to the prospect was restricted therefore the areas geothermal potential remains unknown. The aim of this study was to establish the resistivity structure of this field and to correlate it with the alteration mineralogy and the geological well data from a few wells that have been drilled in this field in the past. An attempt was also made to identify possible locations for future drill holes by considering the outcome of the correlations and hence determine the geothermal potential of the survey area. Modern Magnetotelluric equipment is more efficient in difficult terrain and has a higher resolution power of the ground resistivity in terms of depth. With the transfer of the wildlife in the area and acquisition of the modern equipment, it was now possible to study the area, so as to prospect its geothermal potential. The Magnetotelluric method is more reliable in mapping deeper levels and hence the need to understand the shallow resistivity structure as well, will be made possible by the use of transient electromagnetic method which has proved resourceful in shallow depths.

1.3 Objectives

1.3.1 General objective

To investigate the geothermal potential of the Northwest Olkaria prospect using Transient Electromagnetic and Magnetotelluric methods.

1.3.2 Specific objectives

i. To develop a 1D joint inversion of Magnetotelluric and Transient Electromagnetic maps of the Olkaria North West prospect.

ii. To develop a 1D Iso-resistivity maps of the Olkaria Northwest prospect using magnetotelluric data.

iii. To generate a Magnetotelluric model from Iso-resistivity data of the Olkaria Northwest prospect and evaluate the geothermal potential.

1.4 Hypothesis

i. A 1D joint inversion map of the Northwest prospect cannot be developed using Magnetotelluric and transient electromagnetic data.

ii. 1D Iso-resistivity maps of the Olkaria Northwest prospect cannot be generated using magnetotelluric and transient electromagnetic data.

iii. The geothermal potential of the Northwest Olkaria Prospect cannot be evaluated using 1D-isoresistivity maps of the Northwest prospect.

1.5 Justification

Understanding the resistivity structure of Northwest Olkaria geothermal prospect will give a good understanding of the subsurface and enhance the possibility for the exploitation of this abundant geothermal resource. Retrieval of data within the Northwest field provided a basis for better analysis and interpretation of the resistivity subsurface structure. With better resistivity maps and cross sections, the components of the system and their characteristics were understood. The results locate the up flow, inflow zones and estimated expected temperature distributions to aid future developers in locating sites for production and reinjection wells as well as contributing to the update of the greater Olkaria geothermal area conceptual model. Resistivity maps of the Northwest Olkaria prospect will lead to the discovery of geothermal heat sources within the prospect area. This will be of great economic significance because, it provides an alternative source of energy for the country and encourages the use of clean energy which does not pollute the environment. Increase in the amount of electricity supplied to the national grid may lead to the lowering of the cost of production hence making it possible to achieve the Big four agenda under the manufacturing pillar and consequently lowering the cost of living.

CHAPTER TWO
LITREATURE REVIEW

2.1 Energy

Non-renewable energy sources have zero or a minute rate of replenishment relative to its depletion. Most of these energy sources are converted to usable energy by thermal or nuclear reactions. These energy sources have stored the natural energy flux of Earth's biological and geological past of the formation of elements in the early history of the Universe (Awea, 2015). Renewable energy sources are types of natural energy flux useful for human and regularly occurring on or near Earth's surface and, additionally, useful natural energy stores that are replenished by natural flux within the timeframe of conceivable human use. All known sources originate from, or are close derivatives of electromagnetic radiation of the Sun, the earth's and Moon's gravitational fields and heat radiating from earth's interior. These sources are practically inexhaustible though some sources such as geothermal and ocean thermal energy conversion may become locally depleted by human use at a rate that exceeds replenishment by natural flux (Gritsevskyi, 2017).

2.1.1 Renewable Energy

Renewable energy offers our planet a chance to reduce carbon emissions, clean the air, and put our civilization on a more sustainable footing. They are an essential part of an overall strategy of sustainable development (El Bassam, 2012)**.** They help reduce dependence of energy imports, thereby ensuring a sustainable supply and climate protection. Furthermore, these sources can help improve the competitiveness of industries over the long run and have a positive impact on regional development and employment. They will provide a more diversified, balanced, and stable pool of energy sources.

They are described as naturally replenishing and restore themselves over relatively short periods of time. They are inexhaustible in duration on human-time scales, but limited in the amount of energy that is available per unit time. Such sources include hydro, wave, or tidal, geothermal, solar, wind, and biomass (Ghilardi *et al.*, 2016). However, due to the complexities of how biomass can be produced there is not a clear consensus as to whether it is truly renewable. They do not emit greenhouse gases while producing energy.

2.1.2 Geothermal Energy

Geothermal energy is energy from the heat of the earth's core. Heat has been radiating from the centre of the Earth for 4.5 billion years. At 6437.4 km deep, the center of the Earth hovers around the same temperatures as the sun's surface, 5,500°C. 42 million megawatts (MW) of power flow from the Earth's interior, primarily by conduction (Ľudovít *et al.*, 2010). The constant flow of heat from the Earth ensures an inexhaustible and essentially limitless supply of energy for billions of years to come (National Energy Policy Act, 1992).Geothermal power projects have been developed around the world with a combined capacity of 14,276 megawatts, with the majority located in Asia, North America and Africa (Figure2.1).

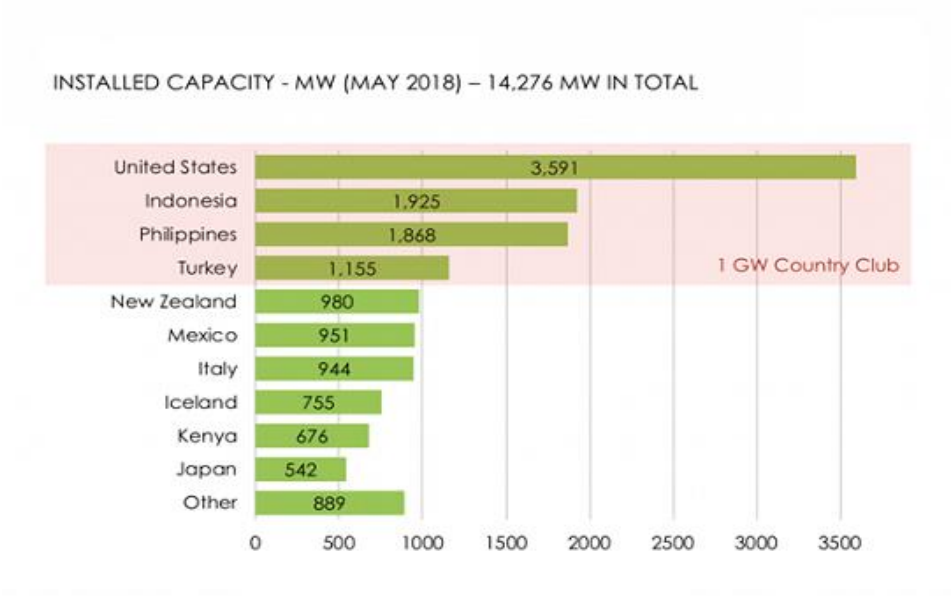

Figure 2.1: Installed geothermal capacity (Khazri, 2018)

2.1.3 Geothermal Resources Identification

Geological, hydrogeological, geophysical, and geochemical techniques are used to identify and quantify geothermal resources. Geological and hydrogeological studies involve mapping any hot springs or other surface thermal features and the identification of favourable geological structures. These studies are used to recommend where production wells can be drilled with the highest probability of tapping into the geothermal resource (Gritsevskyi, 2017). Geophysical surveys are implemented to figure the shape, size, depth and other important characteristics of the deep geological structures by using the following parameters: temperature (thermal survey), electrical conductivity (electrical and electromagnetic methods), propagation velocity of elastic waves (seismic survey), density (gravity survey), and magnetic susceptibility (magnetic survey). Geochemical surveys (including isotope geochemistry) are a useful means

of determining whether the geothermal system is water or vapour dominated, of estimating the minimum temperature expected at depth, of estimating the homogeneity of the water supply and, of determining the source of recharge water.

The aim of geothermal exploration is identification of geothermal phenomena , ascertain that a useful geothermal production field exists, estimate the size of the resource, classify the geothermal field, locate productive zones, determine the heat content of the fluids that will be discharged by the wells in the geothermal field, determine a body of data against which the results of future monitoring can be viewed ,evaluate the pre-exploitation values of environmentally sensitive parameters and determine any characteristics that might cause problems during field development(U.S. Department of Energy, 2010).

2.2 Previous Studies

Extensive geological and geophysical studies have been performed within the Kenya rift these studies have focused more on a broader understanding of the lithosphere and crustal structure and with a minimum focus on individual volcanic systems.

2.2.1 Seismic Studies

The results obtained from the Kenya rift international seismic experiment (KRISP) were probably the most important geophysical models of the rift because they revealed several major features of the rift that provided a model for rifts structures today (Omenda, 2000; Girdler, 2013; Mulwa and Mariita, 2013, 2015). They showed that the crust is approximately 35 km thick in the central section and 22 km northwards towards Lake Turkana (Figure 2.1.) (Simiyu and Keller, 1997, 2001).

The earliest seismic investigation in Olkaria involved passive and active source seismic studies and was undertaken by the United States Geological Survey using an eight-station network. They located 87 events of magnitude 2 and less restricted mainly within a 4 km wide zone parallel to the NS trending Ololbutot fault zone (Mechie *et al.,* 1997). Time distance plots indicated that the area is characterized by a three-layer volcanic sequence of about 3.5-km thick underlain by a granitic layer with a P-wave velocity of 6.3 km/s. Studies done by the Kenya Rift International Seismic Project (KRISP) using the 1985 and 1990 data revealed that the area immediately south of Lake Naivasha is underlain by a 5-layer upper crustal structure (Simiyu and Keller, 1997). Their interpreted model shows a structure with velocities higher than the rift's average.

2.2.2 Gravity Studies

Gravity survey of the shallow crust beneath Olkaria indicated a volcanic zone of three layers that appears down faulted in the Olkaria West area and showing low density. Gravity further revealed the presence of dense dyke material along the Ololbutot fault zone (Simiyu and Keller, 2001). However, it is now known from geology that the N-S Olkaria Hill fault marks a major east dipping fault that has down thrown the Mau formation to more than 3-km in the eastern area. The developed eastern graben was later in-filled with late Pleistocene - Holocene volcanism that was dominated by trachyte, basalts and rhyolite lavas and relatively minor pyroclastic, thus resulting in higher gravity (Omenda, 2000). A Bouguer anomaly map using a density of 2.5 g/cm^3 shows the following features:

1) A NW trending axial gravity high corresponding to the regional geological structure in the Central rift segment.

2) A low gravity anomaly occurs in the west towards the Mau escarpment. Another gravity Low occurs in the eastern Olkaria Domes area and extends to Longonot volcano.

A review of the observed gravity data over each benchmark indicates changes over the years during the monitoring period (Mariita, 2000).

2.2.3 Magnetic Studies

In Olkaria, both ground and aero-magnetic data have been used to investigate the presence of a geothermal resource in combination with gravity. From the aero-magnetic maps several of the anomalies can be clearly correlated with surface expressions of volcanism such as craters, domes or cones, localized basaltic lavas or plugs. From these maps most of the volcanic centers tend to lie in areas with magnetic highs (positives). Sometimes a superimposed magnetic low (negative) exist; but this is generally weak or zero. Mechie *et al.* (1997) analyzed residual draped aeromagnetic data flown at 300m above ground surface within the Olkaria area. Their results showed that the central geothermal area had a positive magnetic anomaly trending NW-SE. This anomaly is superimposed on a broad regional negative anomaly that covers the entire southern Lake Naivasha region and corresponds to normally magnetized rocks. The positive anomaly oriented NW was interpreted to occur in a demagnetized zone corresponding to the main heat source with a temperature above the curie point of magnetite (575^{0}C) and a depth of about 6 km (Ofwona, 2008). A minor trend in the magnetic anomaly is in a NE-SW direction corresponding to the Olkaria fault zone. Bromley interpreted this to represent demagnetized rocks due to alteration by chemical and thermal processes at reservoir depth.

This magnetic anomaly trend is coincident with the deep resistivity conductor and a gap in the micro seismicity.

2.2.4 Resistivity Studies

A resistivity survey of the geothermal field reflected the thermal alteration of the field. High temperatures led to increasing alteration of minerals in the rocks of the subsurface leading to a lowering of resistivity. At Olkaria, direct current resistivity methods have been used for reconnaissance mapping, location of faults for drilling targets and to define the boundaries of geothermal reservoirs (Wamalwa *et al*., 2013). Recent years Transient Electromagnetic (TEM) and Magneto telluric (MT) sounding methods have been favoured due to its simple logistics in the field, cheap cost and high resolution at greater depths. Resistivity data interpretation from the Olkaria geothermal field shows that the low resistivity (less than 20 Ωm) anomalies at depths of 1000 m.a.s.l that define the geothermal resource boundaries are controlled by linear structures in the NE-SW and NW-SE directions (Girdler, 2013; Mulwa and Mariita, 2013, 2015; Wamalwa and Serpa, 2013; Abdelfettah *et al*., 2016). The near surface difference in resistivity is caused by contrasts in the subsurface geology. Drilled wells show that the low resistivity anomalies at 1000 m.a.s.l define a geothermal system with temperatures in excess of 240^0C (Ofwona, 2008). Some of the high resistivity regions coincide with recharge areas associated with NE and NW trending faults that act as conduits for cold water flow from the Rift Valley scarps. The geothermal fluid up-flow zones occur at the intersections of these regional faults in the vicinity of a heat source.

Over one hundred TEM sounding stations have been covered in the greater Olkaria area. The method involved the passage of a large current through an ungrounded loop of wire measuring 300 m x 300 m square. An EM receiver at the center of the square measured the ground TEM response. The data was processed, inverted and produced in apparent resistivity plots in form of contours maps at various elevations. The data shows that the low resistivity anomalies are controlled by linear structures in the NE-SW and NW-SE directions and that the geothermal resource is confined within an area with a low resistivity value of less than 15 Ωm at an elevation of 1400 m.a.s.l. The resistivity was found to be lower around Olkaria West Field (OWF) than the area around East Production Field (EPF) and North East Fields (NEF) (Wamalwa and Serpa, 2013). The near surface difference in resistivity was caused by contrasts in the subsurface geology. An altered thick surficial layer of pyroclastics occurring in the Olkaria West field is the cause of the near surface low resistivity in the field (Omenda, 2000).

Though the MT method has the capability for probing several tens of kilometers, the Magnetotelluric data may be affected by galvanic distortions manifesting as frequency-independent static shifts of the apparent resistivity curves when small-size surficial heterogeneities are present, as can be expected in the weathered and volcanic-covered basement terrain of Olkaria (Abdelfettah *et al.,* 2016). The TEM technique provides a logical shallow-depth (< 1 km) compliment to MT and also serves for correction of MT static shifts. The combined TEM-MT approach has therefore been selected as the technique with optimum potential in Olkaria (Ouma, 2010; Omenda and Simiyu, 2015).

2.3 Magnetotelluric Method

The MT method is an electromagnetic (EM) sounding technique that uses surface measurements of the natural electric (E) and magnetic (B) fields to infer the subsurface electrical resistivity distribution. This method relies on the detection of small potential differences generated by electromagnetic waves propagated from the ionosphere (Ward and Wannamaker, 1983).

2.3.1 Development of Magnetotelluric Method

Due to its simple field logistics and low cost, the MT method is widely used in mineral and geothermal exploration (Christopherson, 2002). Recently, with advances in equipment, data processing and interpretation, MT is more widely used in hydrocarbon exploration. The method is used primarily in areas where seismic exploration is difficult, such as over thrusts and where high-velocity cover such as carbonates and volcanic rocks are present (Kearey, 2013).

When Tikhonov (1950) and Cagniard (1953) proposed the Magnetotelluric method independently, the dependence of MT on natural EM sources quickly attracted geophysicists' attention. Requiring no power source or corresponding control system made it a cost effective exploration technique. In the past fifty years, the Magnetotelluric method has developed both in theory and equipment.

The development of the MT method can be divided into two stages. The first stage was from the early 1950's to the end of the 1970's. During this period, the MT method progressed steadily with the debate on the validity of the plane wave assumption (Wait, 1954; Madden and Nelson, 1964), the introduction of the concept of the impedance tensor (Cantwell and Madden, 1960), the development of remote reference technique (Gamble, 1979), and the application of

1D inversion (Wu, 1968; Oldenburg, 1979). The development was hindered by the lack of innovation in instrumental, data processing and interpretation techniques.

The second stage was from the end of the 1970's to the present day. MT has advanced rapidly with the revolution of digital electronics, new data processing and interpretation techniques. Multi-channel acquisition units have enhanced data quality and efficiency.

2.3.2 Magnetotelluric Theory

Electrical resistivity is the innate property of matter to resist the flow of electrical current. The general definition of specific resistivity is based in Ohm's law (Telford *et al.,* 1990; Paransis, 1997).

$$E = \rho j \quad (1)$$

Where the electric field is proportional to, the current density and ρ is the specific resistivity which relates the two. Its unit is Ohm meters. Resistivity can also be defined through Ohm's law as the proportion between the voltage difference over a conducting wire and the current I through that wire.

$$\rho = \frac{\Delta V}{I} \cdot \frac{A}{l} \quad (2)$$

Where the length of the wire is l and the cross-sectional area is A (Telford *et al.,* 1990; Paransis, 1997; Hersir and Árnason, 2009). While it is perhaps more common to speak of resistivity in geophysical context the reciprocal of resistivity ∂ is conductivity measures in some sense the same thing except from the other end. The unit of conductivity is Siemens per meter.

$$\sigma = \frac{1}{\rho} \quad (3)$$

When dealing with electrical current through a rock matrix the material through which the current is flowing is not uniform. The current will tend to flow through the path of least resistivity and avoid highly resistive material. There are three ways by which electrical current flows through a rock. The first one is directly through the rock matrix itself. However, the rock itself has relatively very high resistivity as compared to the other conduction mechanisms (at typical geothermal temperatures) and acts as an insulator (Telford *et al.,* 1990; Paransis, 1997; Girdler, 2013). If the conduction through the rock matrix itself is nearly negligible then there are two main mechanisms with which electrical current flows in geothermal reservoirs, pore fluid conduction and surface conduction (Hersir and Árnason, 2009). The pore fluid conduction is by dissolved ions in the pore fluid. Surface conduction in which absorbed ions on the pore surface conduct the current.

The natural source of MT fields originates from lightning discharges and magnetospheric current systems set up by solar activity. These sources create a spectrum of EM fields in the frequency band 10^{-4} Hz to 10^{4} Hz that provide information used to delineate structures at depth, from a few tens of meters to the upper mantle (a few tens of kilometers). MT data at various frequencies provide a means to distinguish spatial variations in resistivity vertically and laterally. The EM field penetration, which decays exponentially, is related to the frequency and resistivity of the medium. Higher frequencies map the near-surface resistivity distribution. Lower frequencies that penetrate deeper provide information on deeper structures. (Christiansen *et al.,* 2006). The apparent resistivity for decreasing frequencies thus provides resistivity information at progressively increasing depths and is essentially a form of vertical electrical sounding.

Near surface resistivity in homogeneities has been found to distort the electric field since the field is discontinuous across a resistivity boundary. This distortion is known as static shift. This effect shifts the MT sounding curve (of apparent resistivity versus period) by some constant scale factor. Since the magnetic field is relatively unaffected by static shift, a controlled source magnetic field sounding such as TEM can be used to correct for static shift. The MT sounding curve is shifted vertically so that the high frequency part of the MT curve coincides with the TEM curve. The low frequency MT curve then gives an undistorted view of the deep resistivity section (Jones, 1988).

To understand the Magnetotelluric method, consider a plane EM wave that is incident on the surface of the Earth. The resistivity of the Earth is much lower than the atmosphere, thus an EM signal travels as a wave in the air and diffuses in the Earth. The fundamental equations governing the behaviour of electromagnetic fields are given by Maxwell's equations

$$\nabla . \tilde{E} = \frac{\ell}{\varepsilon} \tag{4}$$

$$\nabla . B = 0 \tag{5}$$

$$\nabla X \hat{H} = \sigma \tilde{E} + \varepsilon \frac{\partial \tilde{E}}{\partial t} \tag{6}$$

$$\nabla x \tilde{E} = -\frac{\partial B}{\partial t} \tag{7}$$

Where E is the electric field strength in *V/m,* B is the magnetic flux density W/m^2, ℓ is the volume charge density in C/m^3, σ is the conductivity in *S/m*, ε is the dielectric constant in F/m, equation 7 can be rewritten as

$$\nabla X B = \mu J + \mu\varepsilon \frac{\partial E}{\partial t} \tag{8}$$

Here J is the current density in A/m^2, and μ is magnetic permeability in *H/m*. Usually the free space values $\mu_0 = 4\pi \times 10^{-7} H/m$ and $\varepsilon_0 = 8.85\ x\ 10^{-11} H/m$ are used in these equations.

Taking the curl of equation 7 and using equation 8, a second order partial differential equation for E alone can be obtained

$$\nabla^2 E = \mu\sigma\frac{\partial E}{\partial t} + \mu\varepsilon\frac{\partial^2 E}{\partial t^2} \tag{9}$$

In the case of a dielectric environment, there is minimal conduction current, and the displacement current dominates. Thus equation 9 can be simplified to the wave equation:

$$\nabla^2 E - \mu\varepsilon\frac{\partial^2 E}{\partial t^2} = 0 \tag{10}$$

In the case of high conductivity, the conduction current dominates and the effect of displacement current can be ignored. Thus equation 9 can be simplified to the diffusion equation:

$$\nabla^2 E - \mu\sigma\frac{\partial \mathrm{E}}{\partial \mathrm{t}} = 0 \tag{11}$$

The Earth can be treated as a region of high conductivity, so the diffusion equation can be used in MT data analysis. For an EM wave with a sinusoidal time variation, the electric field strength can be written as:

$$\nabla^2 E + i\omega\mu\sigma E = 0 \tag{12}$$

Note that due to the transformation of electromagnetic energy into heat, the strength of the fields decreases exponentially with depth. Consider a wave that travels in the Earth with exponential amplitude decay in the *z* direction, equation 12 can be written as:

$$\frac{\partial^2 E}{\partial z^2} + i\omega\mu\sigma E = 0 \tag{13}$$

Where E is the electric field strength at the Earth's surface, equation 12 can be written as:

$$Ek^2 + i\omega\mu\sigma E = 0 \tag{14}$$

Rearranging this formula gives:

$$E(k^2 + i\omega\mu\sigma) = 0 \tag{15}$$

Then solving for *k*:

$$k = \pm(1-i)\sqrt{\frac{i\omega\mu\sigma}{2}} \tag{16}$$

Here *k* is the complex wave number of the medium; *Es* is the horizontal electric field at the surface. So the field propagating in the earth can be written as:

$$E_s = E_0 e^{i\omega t} e^{i\sqrt{\frac{i\omega\mu\sigma}{2}}\mathrm{z}} e^{-\sqrt{\frac{i\omega\mu\sigma}{2}}\mathrm{z}} \tag{17}$$

In equation 18, the exponential term represents the decay of the amplitude as wave travels in the *z* direction. Skin depth is defined as the distance (δ) over which the electric field strength is attenuated by $\frac{1}{e}$ of the original field strength. Since

$$e^{-\sqrt{\frac{i\omega\mu\sigma}{2}}\delta} = e^{-1} \tag{18}$$

The skin depth can be written as:

$$\delta = \sqrt{\frac{2}{\omega\mu\sigma}} \tag{19}$$

An aqueous solution under an electric potential difference, ions are accelerated under the corresponding electric field. These ions are the carriers of the current and their movement determines how strong the current is. However, in the solution these ions are impeded by a drag force based on the viscosity of the fluid. Therefore, the conductivity of the fluid is not only dependent on the number of ions (salinity) but also the viscosity of the fluid. But since viscosity is heavily temperature dependent, so is conductivity of the solution. Since viscosity generally deceases with increased temperature we would expect conductivity to increase with increasing temperature (Figure 2.2) (Dakhnov, 1962).

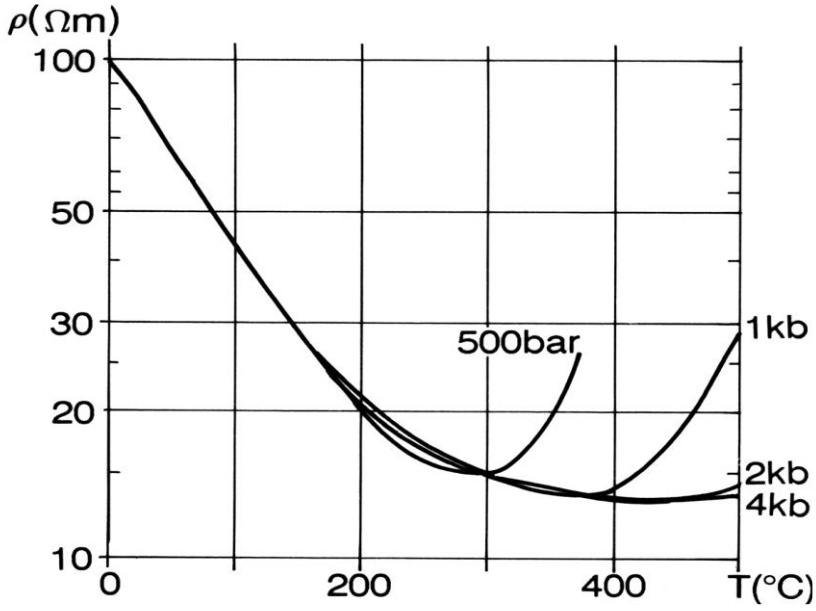

Figure 2.2: Fluid resistivity as a function of temperature for several different pressures (Hersir and Bjornson, 1991)

Resistivity information has for a long time been known to be useful in geothermal exploration. The reason being that, the properties which characterize geothermal systems are directly related to resistivity. These include salinity, temperature, porosity, permeability and

hydrothermal alteration. In high temperature areas the resistivity structure of the sub-surface is often primarily caused by hydrothermal alteration (Tellford *et al*., 1990; Abdelfettah *et al.*, 2016).

This means that information about the resistivity structure of a high temperature area can give indication about the mineral zones of the system due to hydrothermal alteration (Ofwona, 2008). This in turn can give information about other properties such as the spacial variation of temperature within the system. The formation of the alteration minerals is dependent on the primary host rock minerals from which the alteration minerals form, the chemical composition of the geothermal fluid in the system, and the temperature of the system (Paransis, 1997).

This relationship (Figure 2.3) which is an overview of the alteration minerals, their temperature ranges and the respective resistivities commonly seen in Icelandic basalts. However, the temperature inferred from the alteration minerals is not necessarily the current temperature of the system (Tellford *et al*., 1990). It is the alteration temperature, which can be but is not necessarily, the current temperature. The high temperature alteration minerals chlorite and epidote are stable at lower temperatures meaning if they do form in a system of high temperature which then later cools down the resistivity structure remains even if the system is not as hot as the resistivity measurements might indicate (Abdelfettah *et al.*, 2016; Flóvenz *et al.*, 2012).

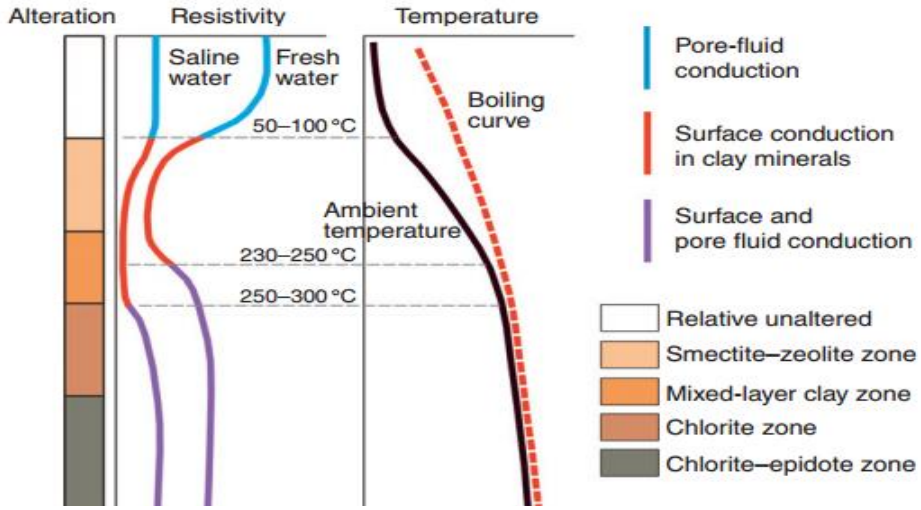

Figure 2.3: Resistivity as function of temperature based on alteration of minerals (Flóvenz *et al.*, 2012).

2.3.3 The Applications of the MT Method

In the early stage, due to the inherent lower resolution compared to seismic and the use of 1D analysis, MT was not suitable for imaging structures in geologically complicated areas. Rather MT was just used in imaging the depth to basement in basins (Kearey, 2013). Even with these limitations, the MT method still achieved significant success in petroleum exploration in the USSR (Berdichevsky and Dmitriev, 2002).

The application of MT in oil and gas exploration in the USSR started in the 1960's. More than 10,000 MT-soundings were carried out within the USSR from the 1960's to the 1980's and the area that was covered with MT amounted to 3 million square kilometers. Because of its low cost, MT was generally used before seismic exploration (Cantwell and Madden, 1960). The major uses of MT were for regional geological study and basin evaluation. The MT data gave a clear image of the topography of basement and yielded enough information to distinguish the structural elements of the basins. The disagreement in the depth of crystalline basement determined by MT data and drilling was often less than 10% (Berdichevsky and Dmitriev, 2002).

In Western Siberian, MT successfully detected a structural high in the Paleozoic basement topography which resulted in the discovery of Urengoy gas field, which is the largest gas field in the world (Berdichevsky and Dmitriev, 2002).

Later, with the rapid development of software and instrumentation, MT has become more useful in exploration. A number of technical advances have been made. The remote reference technique has greatly improved data quality (Gamble *et al.*, 1979). Tensor decomposition can remove three-dimensional distortion (Groom and Bailey, 1989). The Transient EM technique can effectively correct the static shift caused by surficial inhomogenities (Pellerin and Hohmann, 1990). Two dimensional inversions make it practical to image structures in geologically complicated areas (de Groot-Hedlin and Constable, 1990; Smith and Booker, 1991; Mackie and Rodi, 1996). The problem of static shifts can be largely overcome by the two-dimensional regularized inversion (deGroot-Hedlin, 1991).

More portable and reliable digital acquisition systems have been produced by companies such as Phoenix, EMI and Metronix. All these improvements have created a favourable environment for the application of MT in exploration. Since the late 1980's, there has been an increase in the application of MT to hydrocarbon exploration in western countries (Durham ,2017). The applications are concentrated in the over thrust zones that are difficult for seismic exploration due to the high velocity contrast beneath the thrust sheet. Due to a

combination of appropriate source rocks, thermal maturation, and reservoir conditions, overthrust zones are Common targets in petroleum exploration (Picha, 1996). However, in many overthrust zones, the high velocity (older) rocks are thrust to surface, above lower velocity (younger) rocks. This can cause poor quality seismic reflection data in these areas (Watts and Pince, 1998; Watts *et al.*, 2002).

Watts and Pince (1998) show an example of MT exploration in petroleum exploration in southern Turkey. In this case the relatively soft strata, low resistivity deep-sea sediments are intercalated with ophiolitic assemblages, have been thrust over the rigid and high resistivity carbonates. The allochonous sheets in this condition represent a chaotic assemblage of differing lithologies and lead to poor quality seismic data. This has resulted in a resistivity contrast with 1-10Ωm Mesozoic ophiolitic mélange (Kocali and Karadut Formations) over 100 Ωm Martin Group carbonates. Through a comparison of seismic data and MT data, they can interpret the discontinuous seismic reflector (Pellerin and Hohmann, 1990).

Another example is the MT application in sub-thrust petroleum exploration in Northern Greece (Watts *et al*., 2002), where the quality of seismic data is also poor. The MT gave a clear image of the structures there from the resistivity contrast between the carbonates-anhydrite unit (200-2000 Ωm) and the clastic unit (20-100 Ωm). Seismic data acquisition in an area of difficult topography may cost 10 times as much as an MT survey. An MT survey in northern Greece costs 0.11 Million Euro, to cover the same area, where seismic costs 2.375 million Euro (Watts *et al*., 2002). Thus there can be a significant cost/benefit improvement by using the MT method in hydrocarbon exploration in difficult environments. The MT method has been applied in the petroleum exploration in the Papuan fold belt in New Guinea (Christopherson, 1991), where a 1000 m thick Eocene to Miocene massive limestone succession covers a Jurassic-Cretaceous clastic succession, which was the main target of hydrocarbon exploration. Due to the high velocity and karstifing of the limestone outcrop in the fold belt, the quality of seismic data was poor. However, the strong resistivity contrast between the limestone and the underlying clastic succession is favourable for MT exploration. The MT surveys successfully imaged the low resistivity (2.75-7.5 Ωm) Jurassic and Cretaceous clastic succession that beneath the high resistivity (200-400 Ωm) limestone. The MT method also has been used in oil exploration in Minami-Noshiro area in Japan (Matsuo and Negi, 1999). Thrust faults were distinguished by the rapid change of the thickness of the low resistivity layer in the two-dimensional inversion. The resistivity model also gave images of known anticlines and synclines. Three-dimensional inversion has been applied to these data.

Some tectonic studies have also shown that MT data can image thrust sheets. MT data collected in the foreland of the Daxue Shan (northeast of the Tibetan Plateau, china) imaged low angle thrust faults by the resistivity contrast between the overthrust crystalline basement rock (~1000 Ωm) and the underneath basin sediments (10-100 Ωm) (Bedrosian *et al.,* 2001). The high-resolution MT profile of Park *et al.* (2003) yields a resistivity model with a clear image of under thrust sediments at the margin of an intermontane basin in the central Tien Shan Mountains.

The above examples show that the MT method is mature in data acquisition equipment, data processing and interpretation techniques to image structures in overthrust region. Although it has a lower inherent resolution than seismic exploration, its low cost and low environmental impact give it some advantages. There is potential cost benefit if an MT survey is performed before a seismic survey. In an area where seismic exploration is difficult, MT can play a significant role in the reconnaissance stage of petroleum and geothermal exploration.

2.4 Transient Electromagnetic Method

Transient electromagnetic is an active method where a loop of wire is placed on the ground and a current is generated to run in the loop and then suddenly terminated. As Ampere's law describes this current produces around it a magnetic field (hereafter referred to as the primary field) of known magnitude (since the generated current is known). As the current is suddenly terminated the sharp decay of the primary field produces according to Faraday's law a current in nearby conductors, in this case the ground (Telford *et al.,*1990). The current in the ground will seek to mirror the transmitter loop's current in shape and strength as it essentially to maintain the magnetic flux as it was just before the transmitter was turned off. However, the ground current will immediately start to lose power due to ohmic losses (Girdler, 2013). With time, the current and the magnetic field decay and induce currents and magnetic field at greater depths in the ground and diffuse downwards and outwards with time (Figure 2.4). Just like the current in the source loop, the induced current in the ground will produce a magnetic field around itself. As the induced current diffuses downwards and outwards the secondary magnetic field associated with it will change. The way the induced current diffuses is dependent on the resistivity structure of the ground and, therefore, the secondary magnetic field will also depend on the resistivity structure. By setting up a receiver loop on the surface it is possible to measure the rate of decay of the secondary magnetic field since its decay will induce a current in the receiver loop (Tellford *et al*., 1990; Abdelfettah *et al.,* 2016).

Since it is impossible to turn off the current in the entire transmitter loop instantly the current is turned off linearly in a finite short period known as the turn off time (TOFF). Since the strength of the induced current is dependent on the time rate of change of the magnetic flux, the strength of the response is dependent on the TOFF. For this reason, it is desirable to have the TOFF as short as possible for the strongest signal and least amount of noise. The induced voltage in the receiver coil is measured at several points, or time gates, which are defined relative to the zero time when the current becomes zero (end of TOFF), (Africa, 2013). The time gates are equidistant on a logarithmic scale (Figure 2.5).

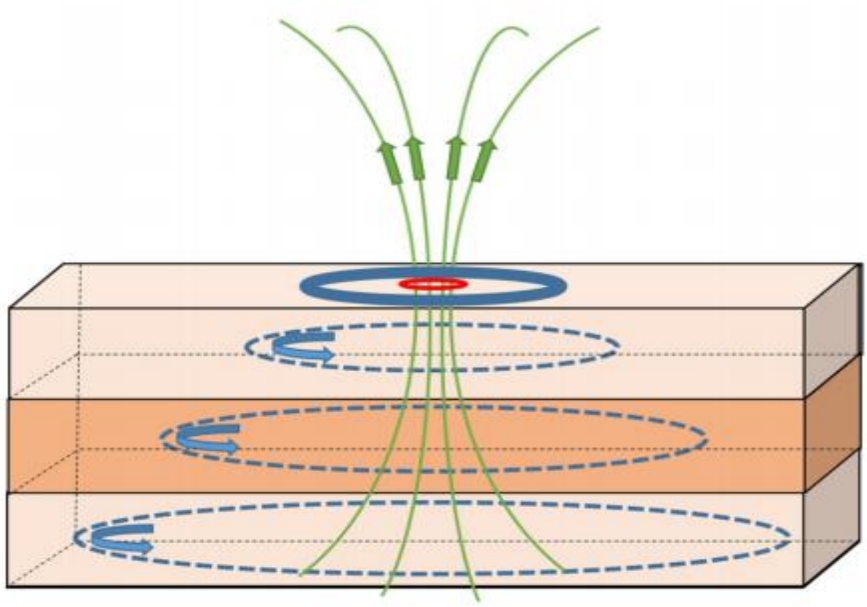

Figure 2.4: Initial current mirrors in the transmitter loop (Africa, 2013)

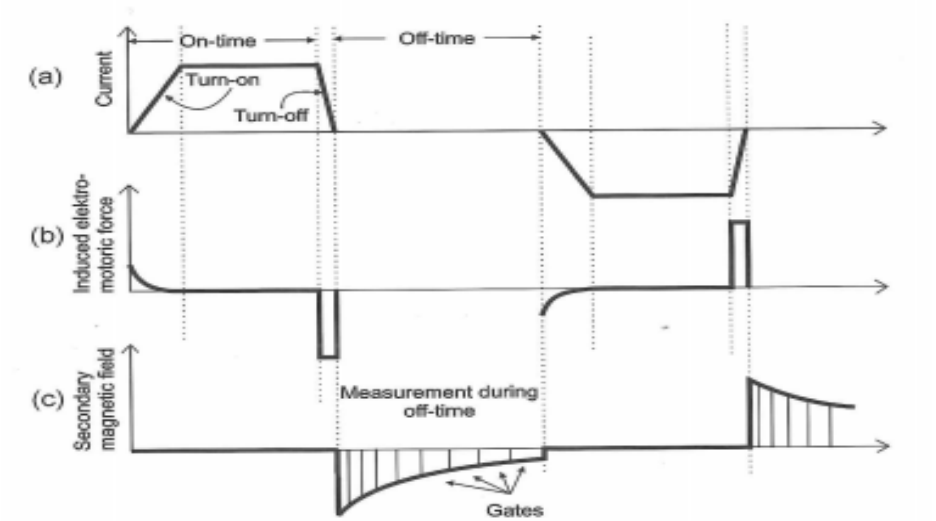

Figure 2.5: Transmitter output and the induced voltage (Christiansen *et al*., 2006).

2.5 Tipper and induction arrows

Both induction vectors and tipper data are MT parameters useful in subsurface body localization and mapping (Fox, 2003). The interpretation of tipper and real induction vectors has its basis in the coordinates of tipper extremes, which are caused by the presence of anomalous bodies (Ingerov *et al*., 2009).

The geomagnetic transfer function between the vertical and horizontal magnetic field components can be expressed as real and imaginary induction vectors. The inclusion of the imaginary induction arrows in the examination gives a quantitative measure of the influence of a three-dimensional conductivity distribution in the investigation area (Marcus, 1999).

According to Schumucker (1970), the real induction arrows point towards a more resistive region, perpendicular to the strike of 23 the lateral resistivity contrast. Furthermore, in the period range of induction, we expect the imaginary arrows to be opposed to the direction of the real arrows. At the period of maximum induction, indicated by the maximum amplitude of the real induction arrows, the imaginary arrows change direction (Marcus, 1999). Simpson and Bahr (1956) have argued that the length of induction arrows is proportional to the intensity of anomalous current concentrations.

2.6 Static Shift Correction

For a layered earth, if two measured apparent resistivity sounding curves XY (electric field parallel to the north) and YX (electric field parallel to the east) have the same shape but exhibit a vertical, parallel displacement but with impedance phase being unaffected, they are probably affected by a surficial body (Khazri and Gabtni, 2018). Hence static shift must be removed before accurate interpretation of deep structures can be made. If YX and XY apparent resistivity sounding are not parallel and the phase is not identical, this indicates an inductive response from 2-D or 3-D structures. Several methods have attempted to remove static shift. Jones (1988) suggested a solution based on shifting the curve into agreement with the model resistivity values of a known layer. Sternberg *et al.,* (1988) have shown the effectiveness of using borehole logged TEM data. One of the most common techniques to deal with this problem is TEM or transient electromagnetic method which depends upon measuring secondary magnetic field and hence is less affected by near surface inhomogenities. Sternberg *et al* (1988), Pellerin and Hohmann (1990) have shown TEM sounding to be quite effective in this respect. Central-loop TEM sounding is commonly used to correct MT static shift because it is less sensitive to lateral resistivity variations than other TEM configurations and the strength

of the induced signal is highest at the centre of the Tx loop. Both central and single loop TEM data for static shift correction for TE and TM modes respectively (Jones, 1988).

2.7 Geothermal resource estimation

The estimation of electrical power for a developed geothermal field may be done by either taking a rule of thumb working from the world average or by the lumped parameter model in which historical productivity is matched with physical observation and is used to predict productivity of fields under similar conditions (Bertani, 2005;Ofwona, 2008).In the case of undeveloped fields where there are either limited or no data available for numerical estimation of their geothermal electrical power potential, a generally accepted method for this estimation involves taking an average power generating capacity of a known geothermal field with similar geological conditions and using it to estimate the potential of an identified prospect area(Durham, 2017). Experience from the nearby Olkaria geothermal field has shown that an average of 15MW is generated using steam collected in one square kilometer of a steam field. The world average production ranges between 1.4 and 13.4 MW per square kilometer (Omenda, 2000).

2.8 Geological and tectonic setting of the Northwest Field

The Great Africa Rift System (GARS) which is a major tectonic structure stretches to about 6100 km from the Red Sea in the north to Mozambique in the south (Shako and Wamalwa,2014). The rift starts from a triple junction which is evident in Ethiopia, at this point two branches are in contact with the Red Sea and the Gulf of Eden and the third is towards the south passing through Ethiopia (Omenda and Simiyu, 2000). Olkaria Geothermal Complex is located in one of the eastern arms of the GARS stretching through Eritrea, Ethiopia, Kenya and Mozambique (Figure 2.6).

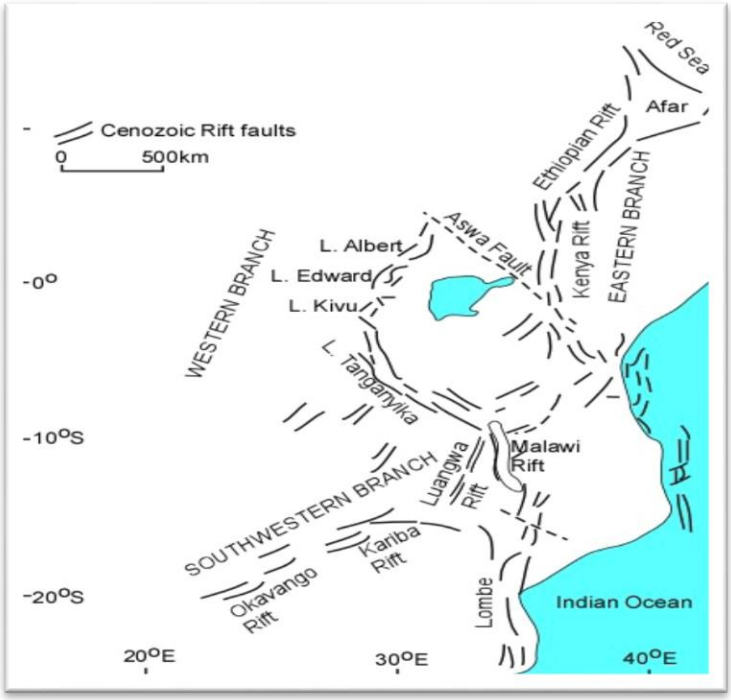

Figure 2.6: Structural map showing the East African Rift System (Omenda and Simiyu, 2000)

The Great Africa Rift system was formed in more or less a linear like zone where the continental plate is being pulled apart with the rifting between widened mantle plume that probably began under east Africa, creating three arms; East Africa Rift, Gulf of Eden Rift and Red Sea Rift (Omenda, 1998). The heat flow from the asthenosphere along the rift zones lead to volcanism and the formation of the domes as can be seen in Olkaria. The eastern branch is believed to be much older and considered to have developed about 13 to 23 million years earlier before the western branch and this was supported by the discovery of preserved vertebrate fossils and volcanic ash which are believed to be about 23 million years old (Ring, 2014).

Geothermal activity in the East African Rift occurs in the form of hot springs, fumaroles, hot and altered grounds, and is closely associated with quaternary volcanoes in the axis of the rifts (Figure 2.7). The association is related to the shallow hot magma bodies under the massifs, which are the heat sources (Simiyu and Keller, 1997, 2001). In the Afar, Ethiopian and Kenya Rifts where the crust has been thinned due to extension, high heat flux is contributed by a shallow mantle. In the less magmatic western branch of the rift, heat sources are a combination of buried intrusions and high heat flux associated with relatively thinned crust (Mechie *et al.*, 1997).

The rifting activity in the Kenya Rift began about 30 million years ago with uplift in the Lake Turkana area and then migrated southward being more intense about 14 million years ago. Formation of the graben structure in Kenya started about 5 million years ago and was

followed by fissure eruptions in the axis of the rift to form flood lavas by about 2 to 1 million years ago. During the last 2 million years ago, volcanic activities became more intense within the axis of the rift due to extension. (Girdler, 2013; Mulwa and Mariita, 2013, 2015; Wamalwa *et al*., 2013; Wamalwa and Serpa, 2013; Abdelfettah *et al*., 2016). During this time, large shield volcanoes, most of which are geothermal prospects, developed in the axis of the rift. The volcanoes include Suswa, Longonot, Olkaria, Eburru, Menengai, Korosi, Paka, Silali, Emuruangogolak and Barrier (Ofwona, 2008).

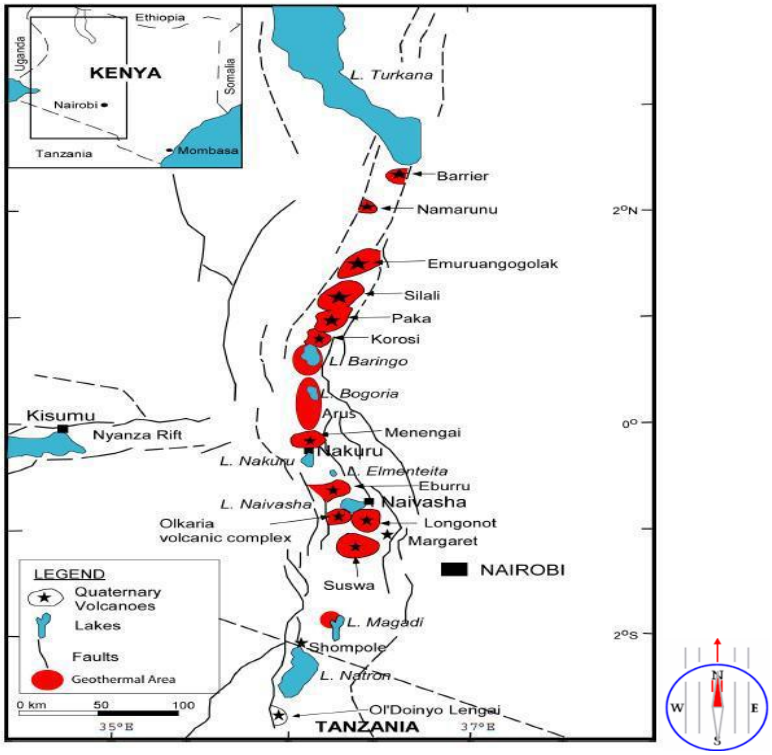

Figure 2.7: Map showing the location of the Greater Olkaria Geothermal Area within the Great Rift Valley of Kenya (Ofwona, 2008)

2.8.1 Geology of Olkaria Geothermal Area

Figure 2.8 shows the rift structure in Kenya along with the distribution of central volcanic complexes in the Eastern African Rift structure (Renaut *et al.,* 2017). Olkaria central volcanic complex is positioned in the part of the rift system. Olkaria similarly has a north-westerly elongation with Longonot volcano aligned in a similar way east south east of Olkaria. This arrangement indicates both NW-SE and N-S structural trends. (KenGen, 2014).

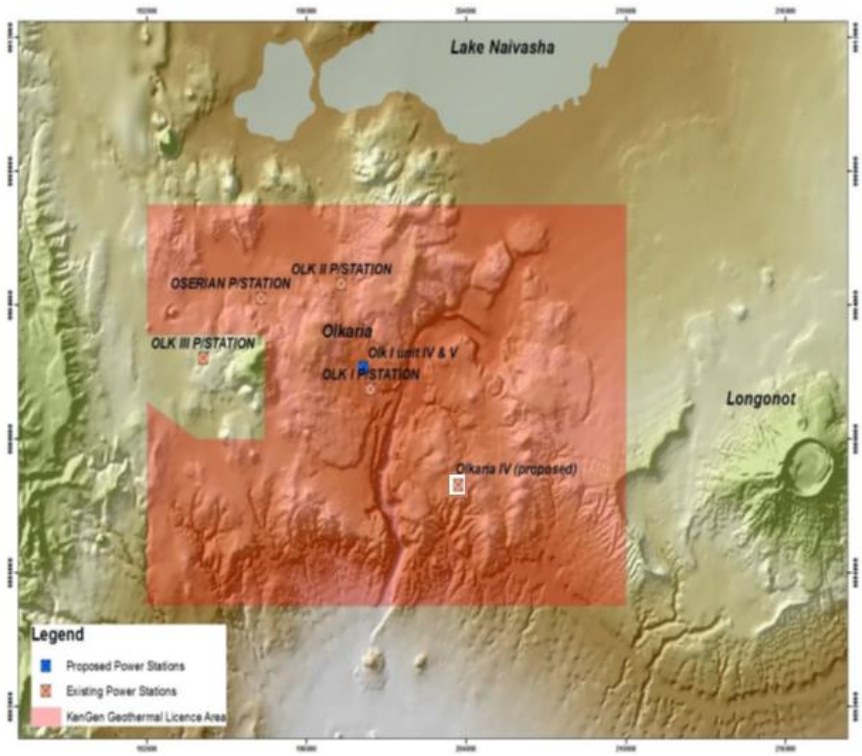

Figure 2.8: Map of the Greater Olkaria Geothermal Area showing KenGen's concessions area and the location of present power plants (KenGen, 2014)

Figure 2.8 shows the overall topographic map of Olkaria and Longonot volcanoes. While Longonot represents a typical conical shaped volcano with a multiple caldera structure and a succeeding build-up of a volcanic cone in the centre, Olkaria has a more complex volcanic build-up. West-JEC (2006) states that although major fractures and faults are observed on surface, their offset and throws are difficult to ascertain due to their limited exposures and loose unconsolidated surface cover and vegetation. The main tectonic structures are aligned N-S and NW-SE, WNW-ESE and NE-SW (Omenda, 2000). The second type of tectonic structures is the ring structures. They are most notable in the south and southeast, but less clear in other areas. From the figure, there exists various interpretations of ring structures. As the focus in the current study is on the NW area, the proposed ring structure is split into an inner and outer ring in the southeast. In the literature these structures are either named calderas or ring structures, where the former indicates the formation of a cauldron, while the latter may not. Apparently, evidence for a cauldron filled up with eruptive material, has not been conclusively identified (Renaut *et al.*, 2017). Comparing Olkaria with other caldera structures in neighbouring volcanic complexes, like Menengai, where multiple caldera structures of variable circumferences are evident (Omenda, 2000; Ouma, 2010; Omenda and Simiyu, 2015). Even Longonot, east of Olkaria appears to have several radial features, which are similar to

those in Olkaria. The meaning of that implies more fracture patterns, which affects and adds to the permeability related structures of the reservoir.

Exposed volcanic formations consist of rhyolitic lavas and pyroclastic rocks, the latter mainly derived from the neighbouring Longonot volcano. The eruptions of rhyolite lavas and domes are strongly related to five N-S tectonic structures, four of which cross the Olkaria ring structure (Ofwona, 2008). They, furthermore, appear to erupt along the ring structures as is particularly evident in the east and south. Further to that is a WNW-ESE structure that passes through the centre of the ring structure and where it crosses the N-S eruption structures, a larger rhyolite effusion is apparently seen. The overall volume of eruptives appears to be small but extensively distributed along the ring structures and tectonic fractures (Wamalwa and Serpa, 2013). The youngest rhyolite, Ol-Butot rhyolite, in Olkaria is dated to about 200 years. Ring or caldera structures are clearly related to magmatic activity, as is evident by the close association of these with magma extrusion (Wadge *et al.,* 2016). Whether the feeders of the rhyolites ascent up vertical "caldera" faults, or if they might be in the form of cone sheets, has not been discussed, but appears to be taken as of the former type (Prodehl *et al.,* 1997).

The volcanic activity may relate to the geothermal one in several ways. It may firstly ascend up from the magma heat source into the geothermal system, up into the cold groundwater system and to surface. The volcanic feeders may secondly be short-lived localized heat sources where the magma consolidates and assimilates it´s heat to the surrounding rock mass (Odera, 2016). It may thirdly form permeable structures for geothermal flow as well as forming barriers to flow oblique to the structure (this condition may though deteriorate with age and later superimposed tectonic activity). The common occurrence of geothermal manifestations along the permeable structures, are clear indications of the ascent of geothermal fluids, at least from the upper part of the system to surface (Abdelfettah *et al.,* 2016).

2.9 Summary of Previous Studies

TEM and MT methods are used extensively in the exploration of geothermal resources because of their advantages in investigating deep subsurface features. The TEM and MT equipment need little space, a small work force and are applicable in difficult terrain. Hersir and Björnsson (1991) describe the application of electrical resistivity methods in the exploration of geothermal resources in Iceland that began in the 1950s. Direct current methods, such as Schlumberger vertical soundings, the dipole-dipole method and head-on profiling were used up to the early 1990s. They have now been replaced by the transient electromagnetic (TEM) and Magnetotelluric (MT) methods.

Olkaria Geothermal Complex is a high temperature geothermal field located within the Kenya rift valley and has been exploited for electricity generation since 1981. A number of exloration methods that included resistivity, gravity, seismic and magnetic have been employed in this field with various levels of success. Overtime, resistivity (mainly MT and TEM) has been preferred due to its ability to identify and delineate geological structures that are directly related to the presence of geothermal reservoirs and systems heat recharge/source. The North West field is part of the greater Olkaria geothermal area. The other sub sections have been exploited and are currently production fields. Previous geophysical studies did not cover the area within the North West field. Hence, a need arises to study this area. This study will employ Magnetotelluric technique to show the resistivity structure of the rocks within the prospect area, which will be used to evaluate the possibility of existence of a geothermal reservoir within the region and the possible capacity

CHAPTER THREE
MATERIALS AND METHODS

3.1 Study Area

Olkaria Geothermal field is a high temperature geothermal resource in the Kenyan Rift Valley which has been used for electricity generation since 1981 (Omenda and Simiyu, 2015). Olkaria geothermal area has been divided into seven development sectors out of which only three have been committed to development. The fields are Olkaria East, Olkaria Northeast, Olkaria South West, Olkaria Central, Olkaria North West, Olkaria South East and Olkaria Domes. The fields are named with respect to Olkaria Hill (Figure2.1) (Omenda, 2000; Ouma, 2010).

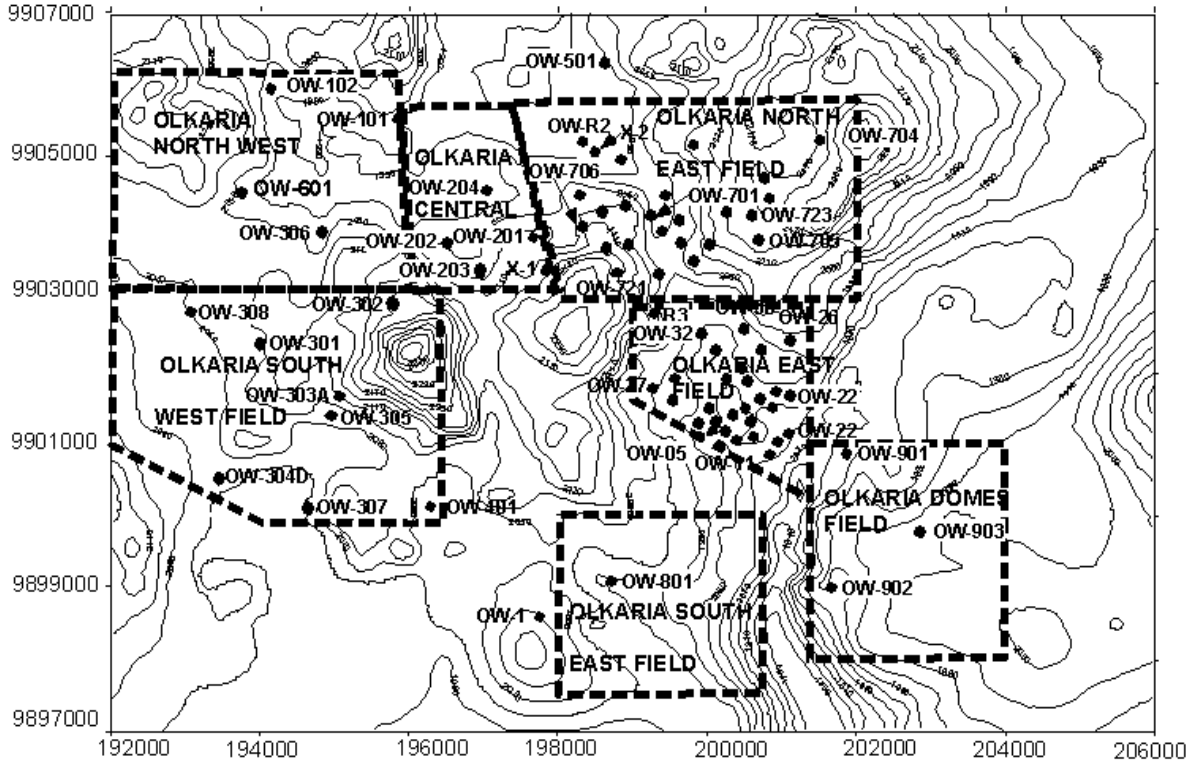

Figure 3.1: Map of Northwest field (Omenda and Simiyu, 2015)

The Northwest Olkaria field (Oserian Sanctuary) is part of the Greater Olkaria Geothermal Area located within the Kenyan rift in Nakuru County. It is bounded by the longitudes 36 ^{0} 15′E and 36 ^{0} 12′E with an estimated area of 30 Km^{2} (Omenda, 2000; Ouma, 2010).

3.2 Transient Electromagnetic Method

In the transient electromagnetic method an electrical current was injected into the ground and the decay of the magnetic field created was measured in order to infer the resistance of subsurface formations. The TEM method effectively resolved the earth resistivity structure down to 2 km. For TEM soundings the Zonge system comprising the following equipment were used; AC Generator (415V), GGT-3 Transmitter, Controller-XMT-16, logger, Geophysical Data Processor (GDP-32[24]), Receiver coil (TEM/3), and Regulator(VR-1) and a GPS.

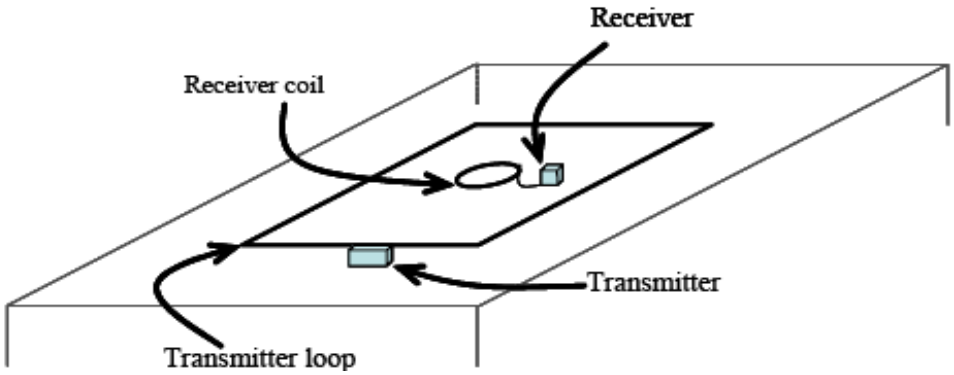

Figure 3.2: Central-loop time domain TEM field layout (KenGen, 2014)

When arriving at site the equipment (GDP-32[24]) was turned on to start heating up the crystal clocks used to synchronize the receiver (TEM/3) and the transmitter (GGT-3). When performing the TEM measurements the transmitter loop was laid down (Figure 3.2) which was done by determining one corner and the center using Pythagoras theorem to determine the distance to half the hypotenuse from the corner, and the direction to the next corner. Since the sides of the rectangular loop are of predetermined length both methods were determined by the square. When the transmitter loop was laid out, the receiver was set at the center of the loop 210 meters (using Pythagoras method to get half the hypotenuse) into the loop (provided the loop was 300m by 300m) in a 45^0angle from one corner. The length of the cable was fixed (at 300 m) and it was laid in an area of approximately 90000 m^2. The receiver coils were sensitive to the quality of the data and it was important that movements were minimized. When both the transmitter and receiver coils had been set measurements were taken.

When starting the power sources both the current and the turns off time in the transmitter were checked (Figure 3.3). The current was measured with the low frequency to get a more stable value, and the turn off time was measured in the high frequency since the turn off time is more important for those measurements. These values were inputted into the receiver

during the measurements. The final measurements for current and turnoff time were made at the end of the measurements. Before measurements were taken, the current and the turn off time were inputted. The receiver coil was then set for the measuring time; for poor quality data, the measuring time was increased to increase the stacking of transients. The number of transients which were bundled together for averaging were displayed on the receiver. This was done three times, two times on the low frequency (4 Hz) and once on high frequency (16 Hz).

Figure 3.3: The transmitter

3.3 Magnetotellurics Method

In the Magnetotelluric technique the fluctuations of the earth's natural electrical and magnetic currents were measured. The lower the frequency, the deeper the penetration. The equipment used for an MT sounding were: An MTU (MT-5A from Phoenix Geophysics, Canada (Figure 3.7), electrical ports (Figure 3.4), electrodes, electric cables, a car battery (12v), a compass and GPS. To ensure good conductivity, the ports were soaked in a solution of sodium chloride.

The three magnetic electrodes were buried at about 1-foot depth and oriented; the four telluric ports were also shallowly buried with a solution of Bentonite. A car battery was used to power the system (Figures 3.5 and 3.6). The MT Unit collected data continuously for at least 18 hours at each MT station).

Figure 3.4: Electrical ports

Figure 3.5: Magnetic electrodes

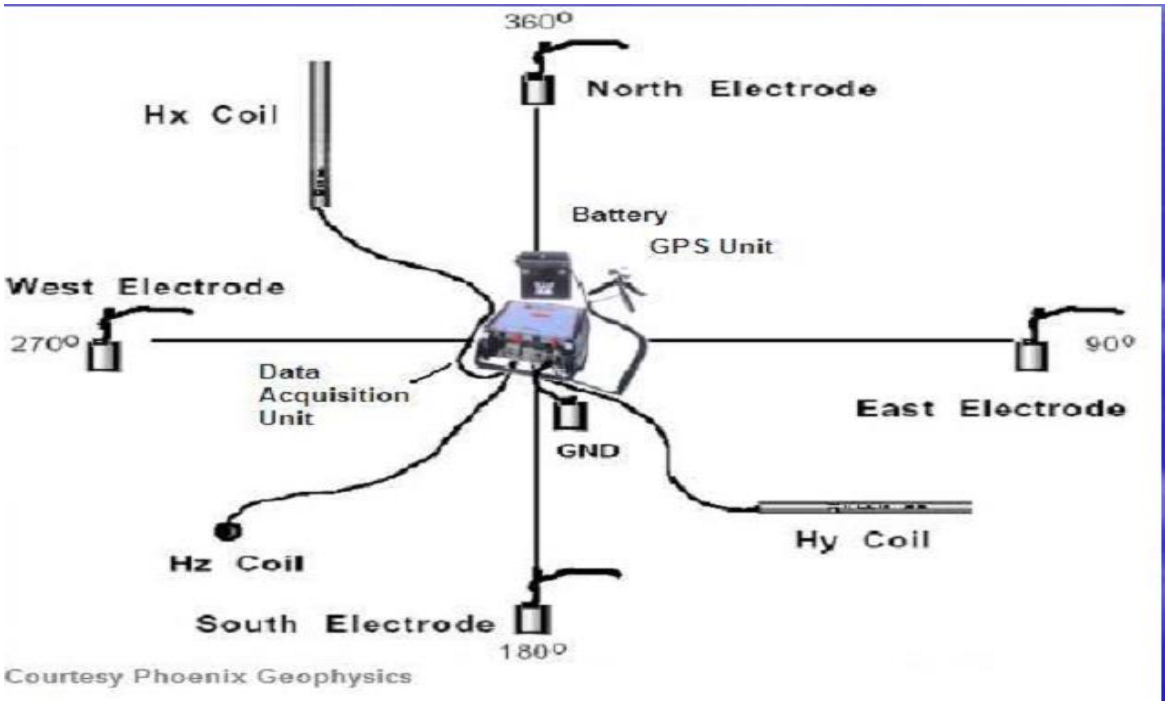

Figure 3.6: A field array for a 5 channel MT data acquisition system (KenGen, 2014)

Figure 3.7: MTU equipment

In this study TEM soundings were carried out at the same stations with MT so that the static shift problem with MT would be resolved using TEM results. These data was used to validate MT data for shallow depths as well as to provide a continuation of deep MT results to the shallow levels.

3.4 Processing of Transient Electromagnetic Data

The raw data from the receiver was processed using a TemX program (Árnason, 2006). TemX computes the forward model using an Anderson style digital filtering technique to carry out the Hankel and Fourier transforms. Fitterman-Anderson style integrations account for the ramp time. Rather than removing effects from the observed data, TemX takes the calculated curves and applies corrections for previous pulse (also known as run-on) and ramp turn-off time. The inversion process uses the Inman style ridge regression approach of nonlinear least squares curve fitting. Prior to inversion, parameters of the starting model are constrained, so that they will not be adjusted by the inversion algorithm, or so that their adjustment is limited (Figure 3.8).

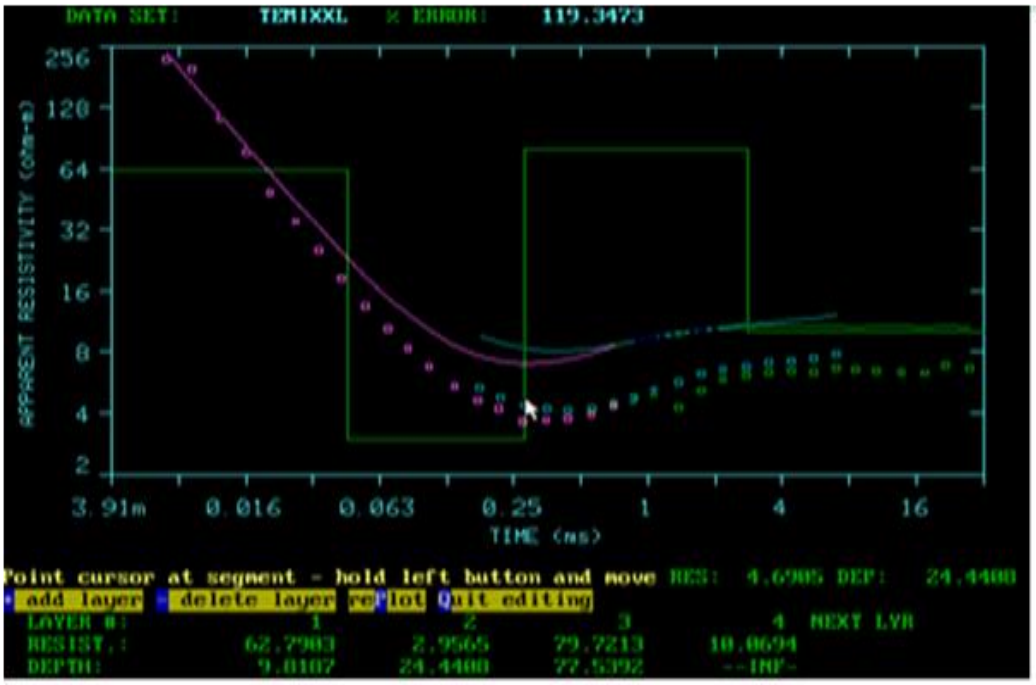

Figure 3.8: Processing screen from TemX showing interactive model construction.

The software downloaded the files from a sounding; normalized the parameters from the measurement such as transmitter current, the gain used in the receiver and the effective area of the antennas. TemX then displayed all the data graphically allowing the examination of the data and removal of outliers. The main graphical window of TemX has two graphical panels (Figure 3.9).

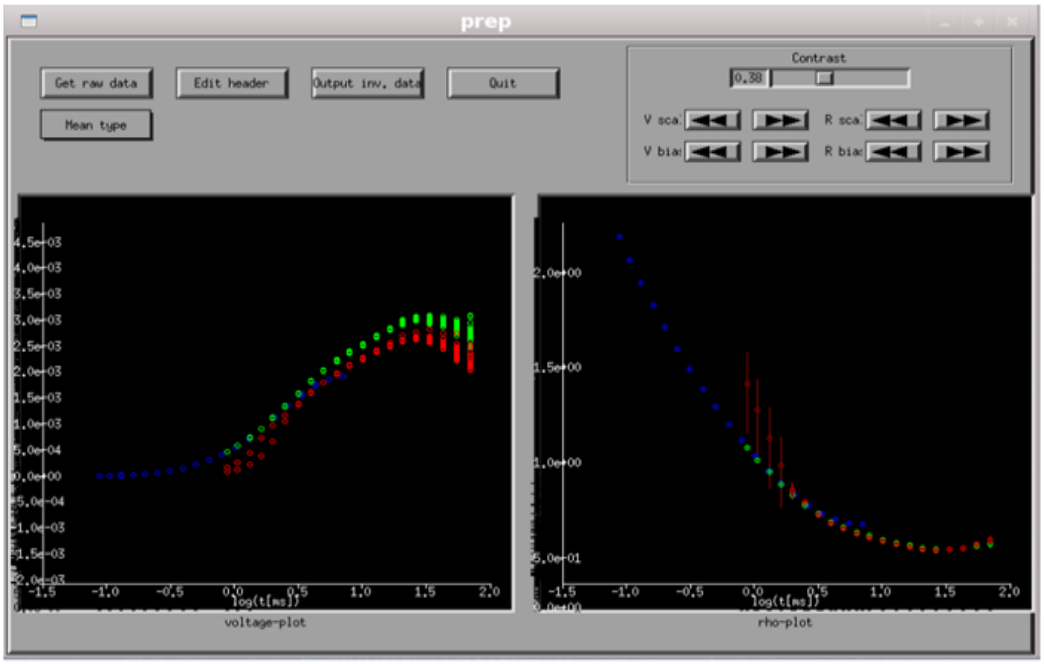

Figure 3.9: The main graphical window of TemX. Voltage data on the left and apparent resistivity on the right (Arnason, 2006)

The left panel shows normalized voltage multiplied by log time. The right one shows apparent resistivity against log time. Four data points have been excluded from this data set. The four data points were omitted because they were significantly above the otherwise relatively smooth curve the rest of the data shows. The program then calculated averages of the datasets and late time apparent resistivity. When the data had been processed using TemX they were ready for modelling. The modelling was done using another program called Temtd, which is an inversion algorithm used for creating a 1D horizontal layered earth model that best fits the data (Árnason, 2006). The method of Occam inversion was used.

The Occam inversion uses a number of layers each of equal thickness (on a logarithmic scale) and only varies the value of resistivity in each layer. Figure 3.10 shows the model which best fits the data.

The model is in green with 50 layers, the measurements are the red dots (resistivity as a function of the square root of time) and the calculated response from the model is the solid black line. On the horizontal axis is depth in meters and the vertical axis is the resistivity. The chi (or χ) parameter is a measure of how accurately the model fits the data, the lower the chi value the better is the fit (Árnason, 2006).

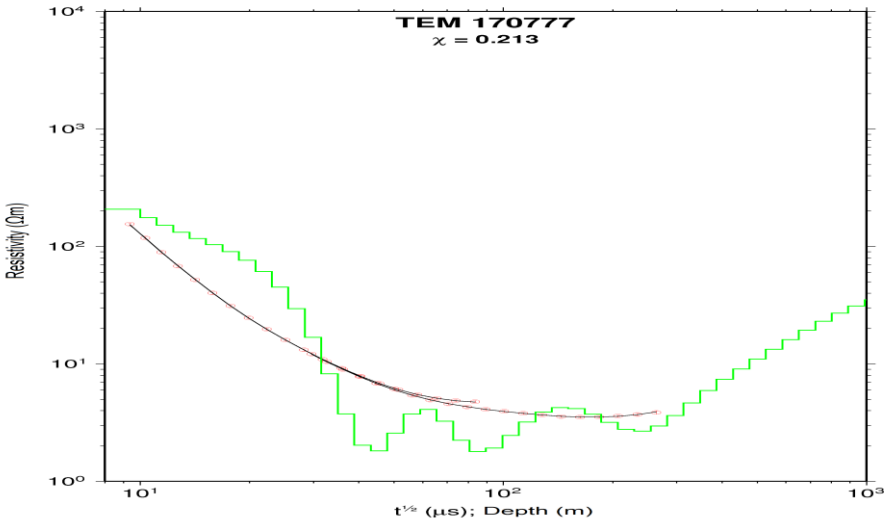

Figure 3.10: A log-log graph of Occam inversion modelling

3.5 Processing of Magnetotelluric Data

The data was acquired using a 5-channel MT data acquisition system (MTU-5A) from Phoenix Geophysics. The instrumentation consisted of a data recorder, induction coils, non-polarizing electrodes, Global Positioning System (GPS), 12 V battery, flash memory for data storage, and telluric and magnetic cables. The layout was such that the electric dipoles were aligned in magnetic North-South and East-West, respectively, with corresponding magnetic sensors in orthogonal directions; the third magnetic coil was positioned vertically in the ground as demonstrated in figure 3.6. Before data acquisition, a start-up file was prepared with parameters like gains, filters, time for data acquisition and calibrations for both equipment and the coils and stored on a flash disk in the equipment.

The ground contact resistance was generally measured to gauge the electrode coupling to the ground. An anti-aliasing low-pass filter was used as well as a high-pass filter with a corner frequency of 0.005 Hz to remove the effect of self-potential from the electric dipoles. The electric field was measured by lead chloride porous pots and the magnetic sensors were buried about 20 cm below the surface to minimize the wind effect as the coils were sensitive to any form of movement.

In the region, MT was deployed with the intention of probing to greater depths; thus, the acquiring system was left overnight so as to collect data for long periods of 20 hours or more and also to take advantage of the stronger signals usually available in the late hours of the night. This helped in getting the low-frequency signals, hence achieving the objective of deep probing (the lower the frequency, the greater the depth of investigation). Over 50 MT

soundings were carried out in the area but only 50 soundings were considered for this particular report, this was because only MTs with corresponding TEMs were considered.

Time-series data from the MT equipment were processed by the SSMT2000 program, provided by the equipment manufacturer, Phoenix Geophysics of Canada (Figure 3.11). First the parameter file was edited to reflect the data acquisition setup and then the resulting time-series data were transformed to the frequency domain using fourier transforms. From the Fourier transform band averaged cross-powers and auto-powers were calculated using the robust processing method.

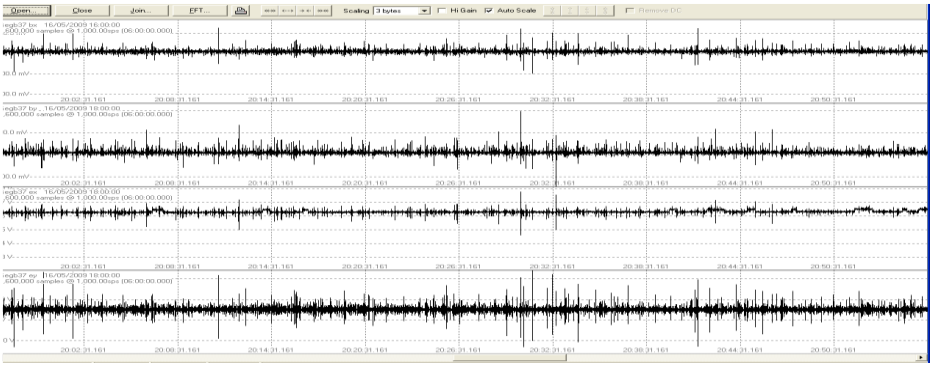

Figure 3.11: Time series data downloaded from SSMT 2000 (NWMT 58)

The cross-powers were then graphically edited by the MT editor to remove the noisy data points and evaluate smooth curves (coherent) for both phase and apparent resistivity (Figure 3.12).

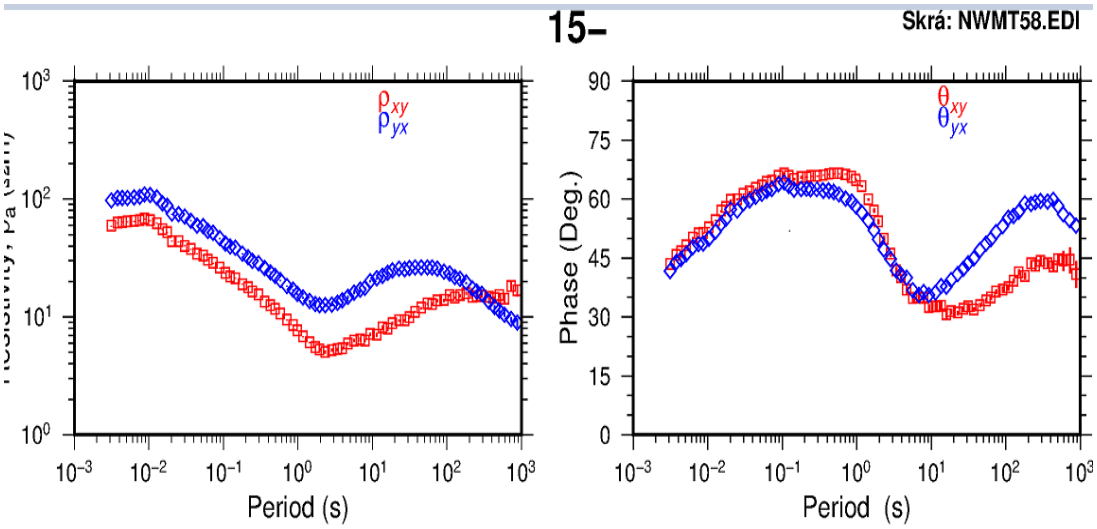

Figure 3.12: Processed MT apparent resistivity and phase curves of an MT sounding in the NW Olkaria field

The SSMT2000 was used for configuring MT instrumentation and parameters. The MT Editor Programme accepted MT plots output by SSMT2000, merged the cross powers and

displayed M T parameters graphically (Boashash, 2015). It also enabled elimination of cross powers from the calculations and hence the possibility of editing out poor quality data (Figure 3.12).

The primary objective of editing was to create a smooth resistivity curve by eliminating those cross powers that had moved too far from the mean by noise and related effects. Though it was possible to eliminate data points from being considered, the software did not delete them completely. It placed a mask on those unwanted cross powers, allowing reversion to the original data at any time. Figure 3.12 indicates that there is a 1D response with decreasing resistivity for periods below 1s. The final cross-powers and auto-powers, as well as all relevant MT parameters calculated, were stored in EDI files which are the industry's standard. These EDI files were then used as input for the Linux program TEMTD where they were used for joint inversion with TEM (Boashash, 2015).

A well-established method for static shift correction of MT data was then used with TEM (Stenberg *et al.,* 1988; Pellerin and Hohmann, 1990). The imported 1D model was used to calculate a forward MT response. The observed apparent resistivity curve was then shifted along the resistivity axis to coincide with the values suggested by the TEM response (Khazri and Gabtni, 2018).

3.6 Joint Inversion of TEM and MT Data

Geophysical inversion is a tool with which we can use to recover the subsurface distribution of a physical property from field-collected data using one or more inversion algorithms. The 1D joint inversion was performed simultaneously for both TEM and MT data by fitting one inversion on both data sets to obtain one model. This is achieved by use of an algorithm which determines the appropriate shift factor to be used to constrain the MT data to fit the TEM response. Both the MT and TEM data collected on approximately the same location are brought together in a joint inversion where TEM 1D inversion obtained earlier was used for static shift correction on MT data. The TEMTD program was used to invert MT apparent resistivity and phase derived from the rotationally invariant determinant of the MT tensor elements (Figure 3.13). In the joint inversion, one additional parameter was also inverted for, namely a static shift multiplier needed to fit both the TEM and MT data with the response of the same model, (Árnason, 2006). The red diamonds are the measured TEM apparent resistivities and blue squares are the MT apparent resistivities and phase. Solid lines show the response of the resistivity model to the right. The shift multiplier is shown in the upper right

hand corner of the apparent resistivity panel. The best fit for this data was achieved with a shift parameter of S = 2.13 which means the MT curve was shifted upwards.

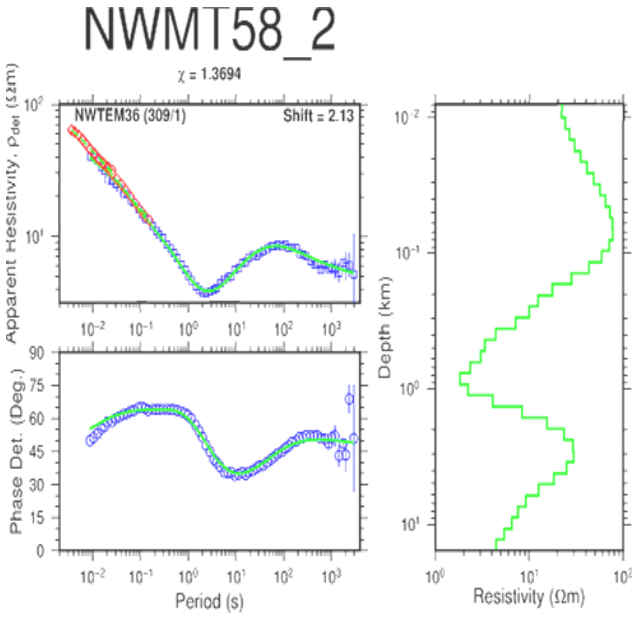

Figure 3.13: Joint 1.D inversion of TEM and MT soundings (NWMT58_2)

A number of cross sections were made to display the result of the 1D inversion of the MT and TEM soundings. The programme TemTD performed 1D Inversion with horizontally layered earth models of central-loop Transient Electro-Magnetic and Magnetotelluric data. It was used to invert only TEM or MT data and also for joint inversion of TEM and MT data, in which case it determined the best static shift parameter for the MT data. For TEM data, the programme assumed that the source loop was a square loop and that the receiver coil/loop was at the centre of the source loop. The current wave form was assumed to be half-duty bipolar semi-square wave (equal current-on and current-off segments), with exponential current turn-on and linear current turn-off. For MT data, the programme assumed standard EDI of impedance and/or apparent resistivity and phase data. The programme is written in ANSI-C and runs under UNIX/LINUX operating systems. It uses the g.n.u plot graphics programme for graphical display during the inversion process (Árnason, 2006).Joint inversion of MT and TEM data was performed to deduce 1D smooth models of the subsurface resistivity structure as well as resistivity isomaps at different depths, elevations and periods/frequencies.

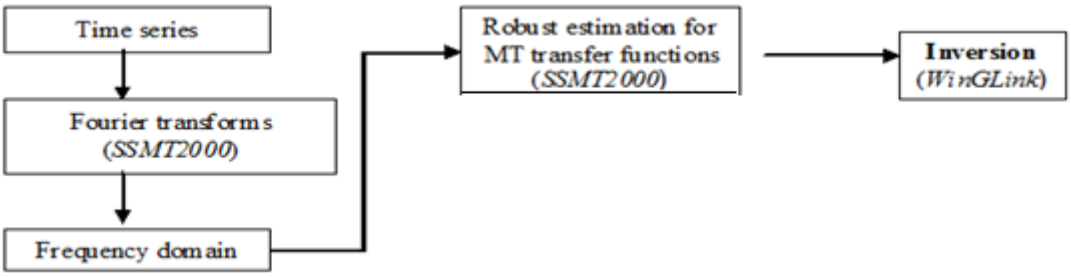

Figure 3.14: Flow chart of data processing steps (Árnason, 2006).

CHAPTER FOUR
RESULTS AND DISCUSSION

4.1 Introduction

This chapter presents the results of the geophysical work performed in Olkaria Northwest in the Greater Olkaria Geothermal Area using Magnetotelluric and Transient Electromagnetic methods. The surveys involved data acquisition, processing and interpretation using a one dimensional joint inversion of the data sets based on a nonlinear least-squares inversion of the Levenberg-Marquardetcode, (Árnason, 1989) and the results are presented using both iso–resistivity maps at different elevations and resistivity cross-sections along selected profiles.

The EM data that were used in this project were 50 MT soundings and 47 TEM soundings were collected for deeper underlying structures. The joint processing technique was used to correct the static shift problems encountered by MT.

In this study a total of 47 TEM (Figure 4.1) and 50 MT soundings spread over an area of about $30km^2$ were carried out in Olkaria North West using the central loop TEM configuration which involved transmission of a half-duty (50% duty circle) square wave current into a transmitter loop at frequencies of 16Hz and 4Hz using Zonge TEM system from Zonge Engineering (USA) that is comprised of a transmitter, 24 bit multifunction receiver, voltage regulator, $1.0mm^2$ transmitter cable and a receiver coil with a dipole moment of about$10000Am^2$ .In the field setup, depending on the available space either a 300 x 300 or a 200 x 200 transmitter loop was used to transmit the half duty current wave at the frequencies stated above. In both cases the transient signal was recorded at the center of the loop at time intervals with logarithmically spaced- sampling time gates after the current turn-off.

4.2 1D Joint Inversion of Magnetotelluric and Transient Electromagnetic Data

The TemX program was used to process the raw TEM data, the program read the files from the soundings, normalized the parameters such as transmitter current, gain used in the receivers and the effective area covered by the antennas. It then displayed the data graphically allowing examination and removal of outliers. The program then calculated the averages of the data sets and the late time apparent resistivity. The TEM data was then inverted using layered models as well as the initial model for Occam inversion. (Figure 4.2)

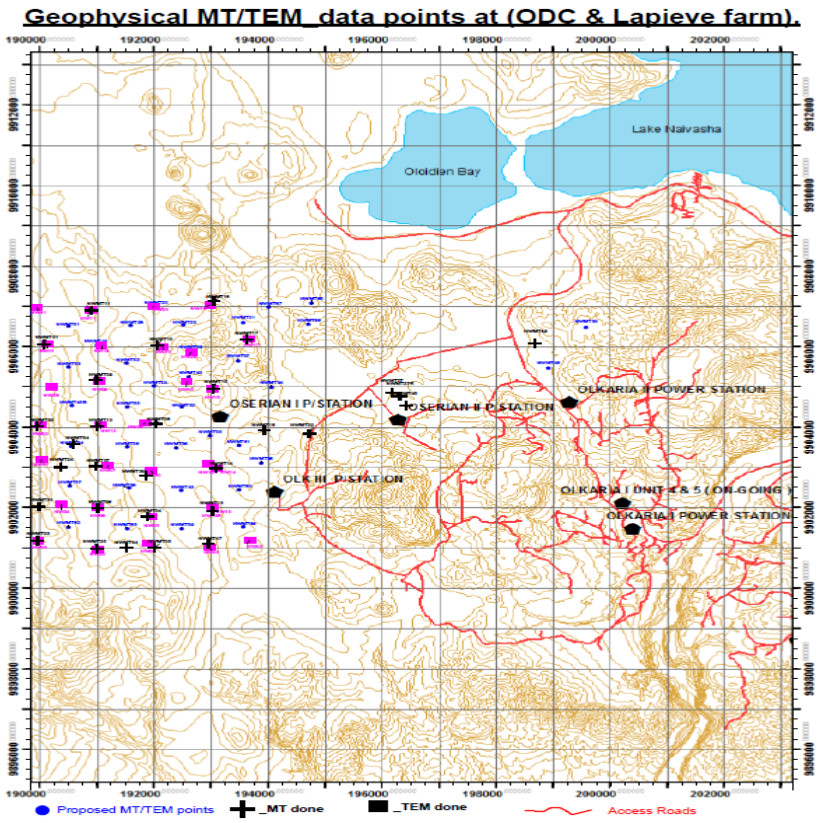

Figure 4.1: Map of TEM and MT data points

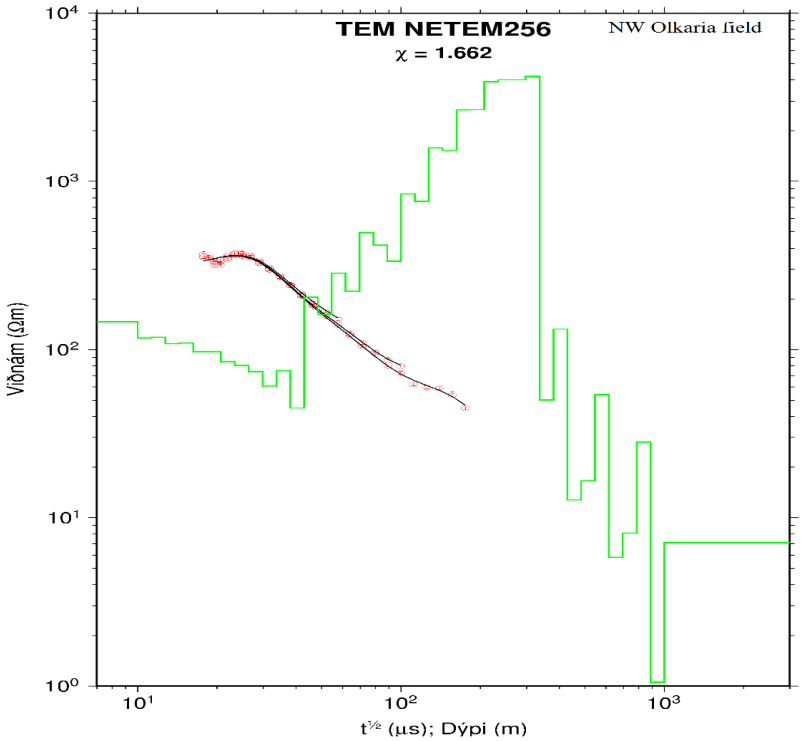

Figure 4.2: ID Joint inversion of MT and TEM for Occam modelling

4.3 1D Iso-Resistivity Maps of the Olkaria Northwest Field

1D Iso-resistivity maps were developed by merging 1D cross-sections plotted from 1D inversions by petrel.

4.3.1 1D Cross-sections

Resistivity cross-sections are plotted for results obtained from 1D inversion by petrel program, developed by Slumberger (https://www.software.slb.com/products/petrel). The programme calculates the best line between selected soundings on a profile, and plots resistivity iso-lines based on the 1D model for each sounding. It is actually the logarithm of the resistivity that is contoured so the colour scale is exponential but numbers at contour lines are actual resistivity values. Several cross-sections were made through the survey area and profiles were positioned perpendicular to the inferred geoelectrical strike.

4.3.2 NS Moving WE Direction

These profiles trend in the NS direction and show the variation of conductivity from West to East at different depths above sea level (figure 4.3). The resistivity structure generally shows a four-layer high-low-high-low resistivity trend. The topmost >30 ohm-m resistivity layer coincides with the unaltered formation and the superficial deposit on the surface. Beneath this thin high resistivity layer is a thick layer of a very conductive ≤6 ohm-m dome-like layer that extends up to 1900 m.a.s.l coinciding to a low medium temperature alteration and is interpreted as the clay cap. It is a zone that is dominated by conductive alteration minerals such as smectites and zeolites. Beneath the base of this conductor is a resistive >15-50 ohm-m which is associated with the high temperature secondary minerals such as epidote, chlorite and biotite present in the reservoir. Beneath the resistive layer is another high conductivity layer extending to about 6,000 m.b.s.l and it is associated with the heat source.

The cross-sections are disecting the area in N-S direction (Figure 4.4) across the production field of Olkaria. The resistivity structure generally shows a four-layer high-low-high-low resistivity trend. There is a very good agreement between the resistive anomalies and the most productive wells. The deep wells in Domes and Olkaria Central field correspond to the deep high resistivity anomaly defined by MT data, while the low productive wells fall within the generally conductive shallow subsurface layer.

The shallow structure reflects the lithological response of shallow formations, which are quite conductive interpreted to be due to the presence of low temperature alteration

minerals. It is clear that the low resistivity cap on the western side is different from the high resistivity on the Eastern side.

The western side is conductive and thicker than the eastern side. Lack of alteration mineralogy of the drilled wells to the West (Oserian Wells) has made it deficult to correlate the alteration mineralogy with resistivity. The alteration mineralogy on the Eastern part of the study area is in agreement with resistivity. However, where geological information is available and the geometry of the formations is known, the two different effects can be separated.

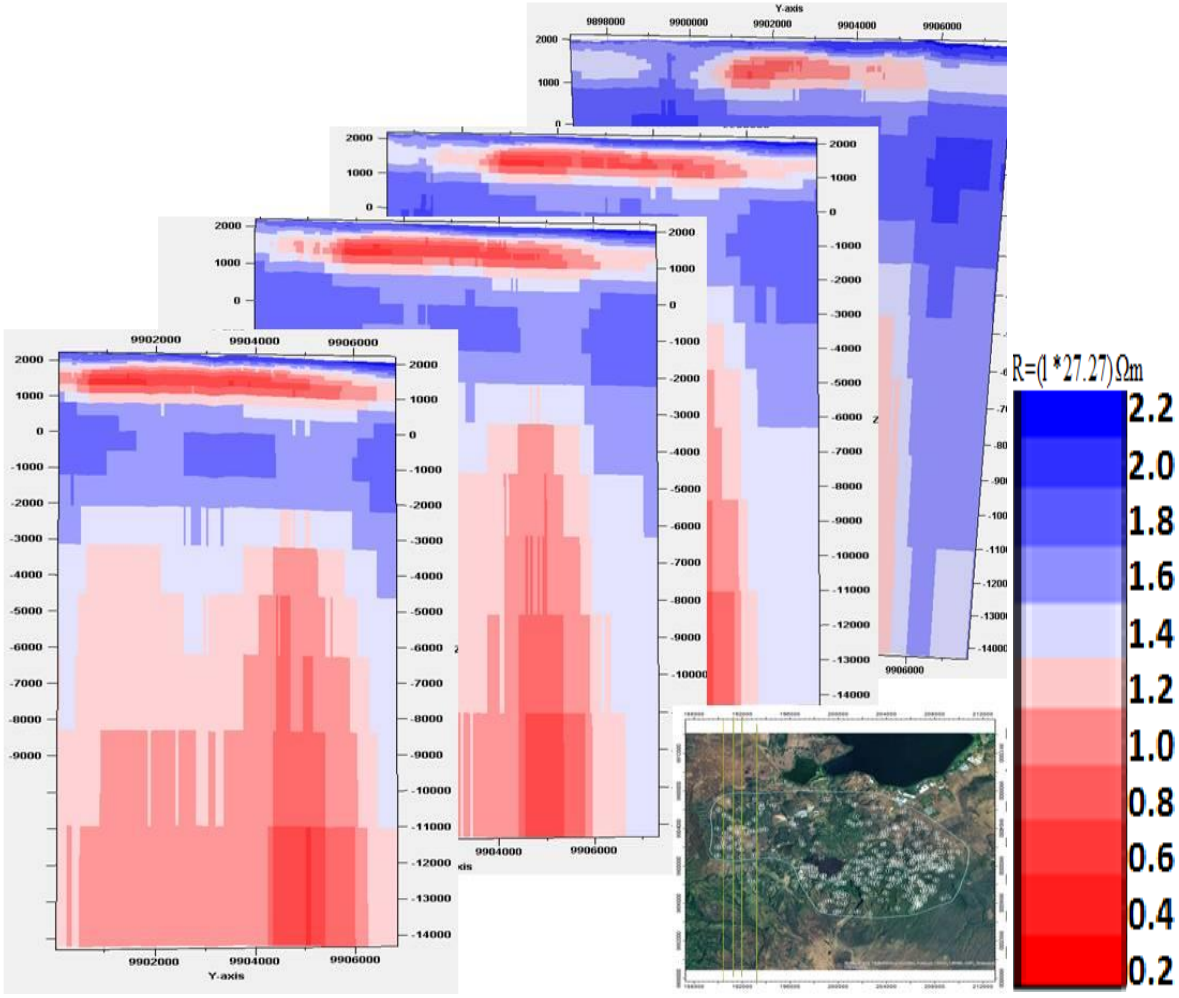

Where R=(ℓ*27.27) ohm-m

Figure 4.3: Vertical cross sections indicating resistivity against depth in the NS direction. The google map depicts the directions of the profiles on which the cross sections are drawn.

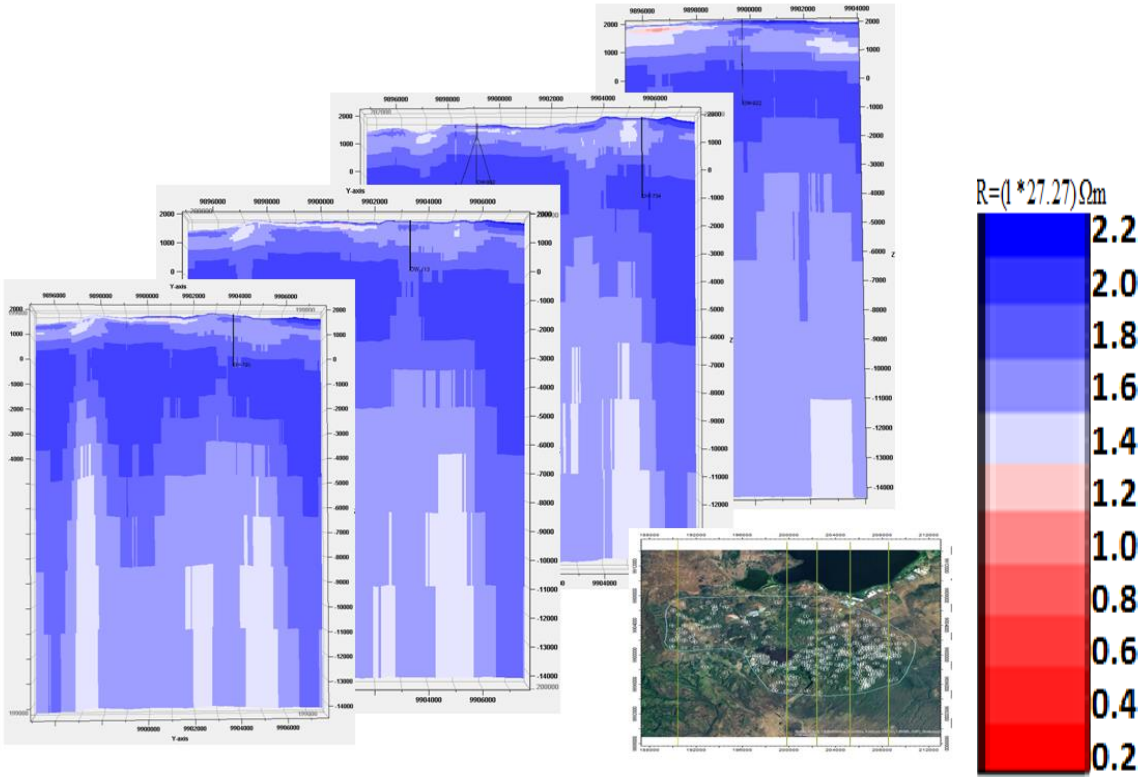

Figure 4.4: Vertical cross-sections indicating resistivity against depth in the NS direction at 6000 m.b.s.l4.2.2 E-W Cross-Sections (moving from North-South)

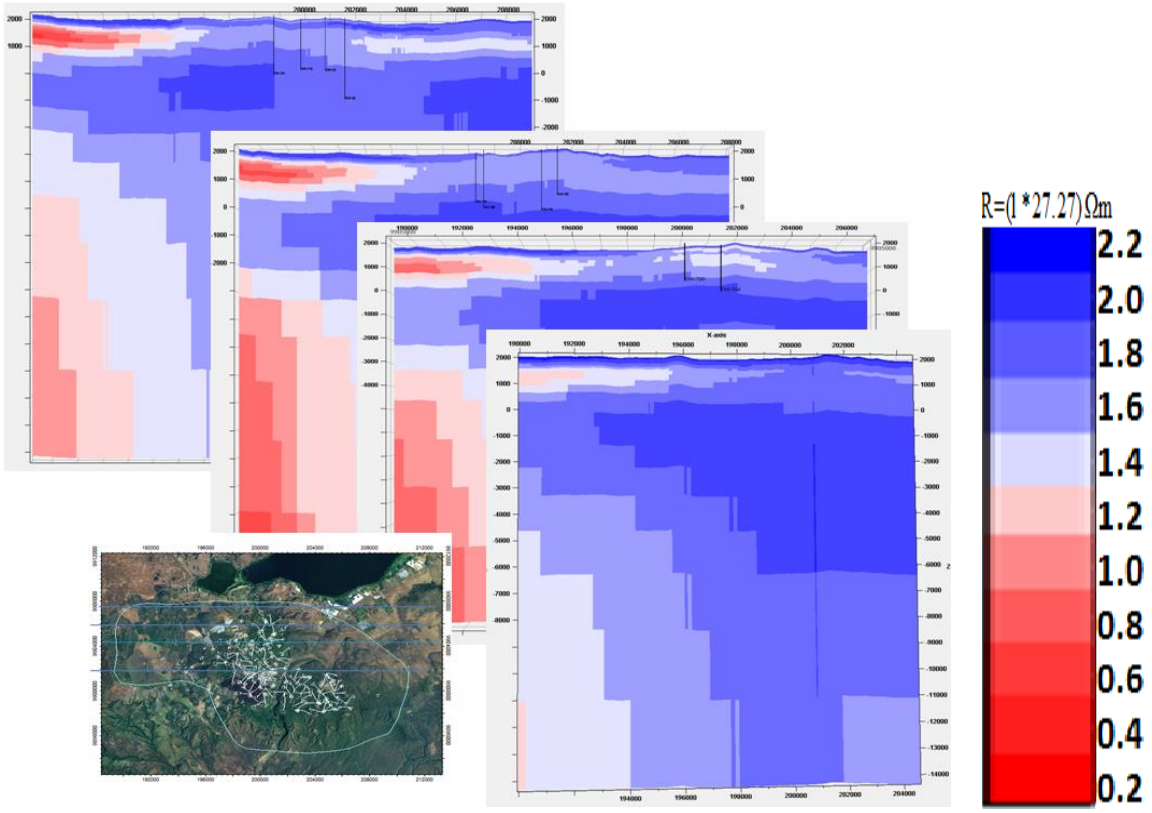

Figure 4.5: Vertical cross sections indicating resistivity against depth in the W-E direction at 6000 m.b.s.l.

The East-West profiles presented in Figure 4.5 are running W-E direction covering about 20 km. The resistivity structure generally shows a four-layer high-low-high-low resistivity trend. The high resistivity near surface is uniform along the profile and is associated with the presence of unaltered formations and superficial deposits. This is underlain by a low resistivity which is not uniform along the profile. The western side possesses a highly conductive and probably much more conductive than the Illitic clays and other high temperature mineralization that occur above 200°C. Therefore, in most high temperature geothermal systems, there is a characteristic clay "cap" that forms above the main high temperature reservoir and often on the sides of geothermal systems, particularly in outflow areas. This clay cap is the most dominant feature seen by resistivity surveys and so provides a useful indicator of the location and extent of the underlying higher temperature reservoir. The clay cap layer to the western side is thicker than the clay cap to the eastern side which leads to change in the casing design and depth of drilling to accommodate the high temperature zone. The base of the clay cap usually marks the transition to high temperature reservoir (or, at least, reservoir at temperature greater than 200°C) and can be treated as a thermal indicator. The top of the cap typically marks the upper extent of thermal activity (about 50°C). Underlying the clay cap is resistive layer interpreted to be the due to the presence of high temperature alteration and interpreted as the main reservoir. This layer is very thin to eastern side and apear to be deep but the same layer is very thick along the profile to the east and very deep which might mean the reservoir to eastern side is thin and very deep. The conductive layer below the main reservoir system can be interpreted to be due to the presence of heat source.

4.4 1D Iso-Resistivity Maps and 1D Magnetotelluric Model of Olkaria Northwest Field

Iso-resistivity maps are made by a program known as TEMRESD which generates iso-resistivity maps at fixed elevations derived from the 1D Occam models (Eysteinsson, 1998). The resistivity is contoured and coloured in algorithmic scale. The general elevation of the area is just above 2000 m.a.s.l. In this section, iso-resistivity maps are presented from 2000m.a.s.l. down to 6000 m.b.s.l. The maps show that resistivity varies considerably both laterally and with depth.

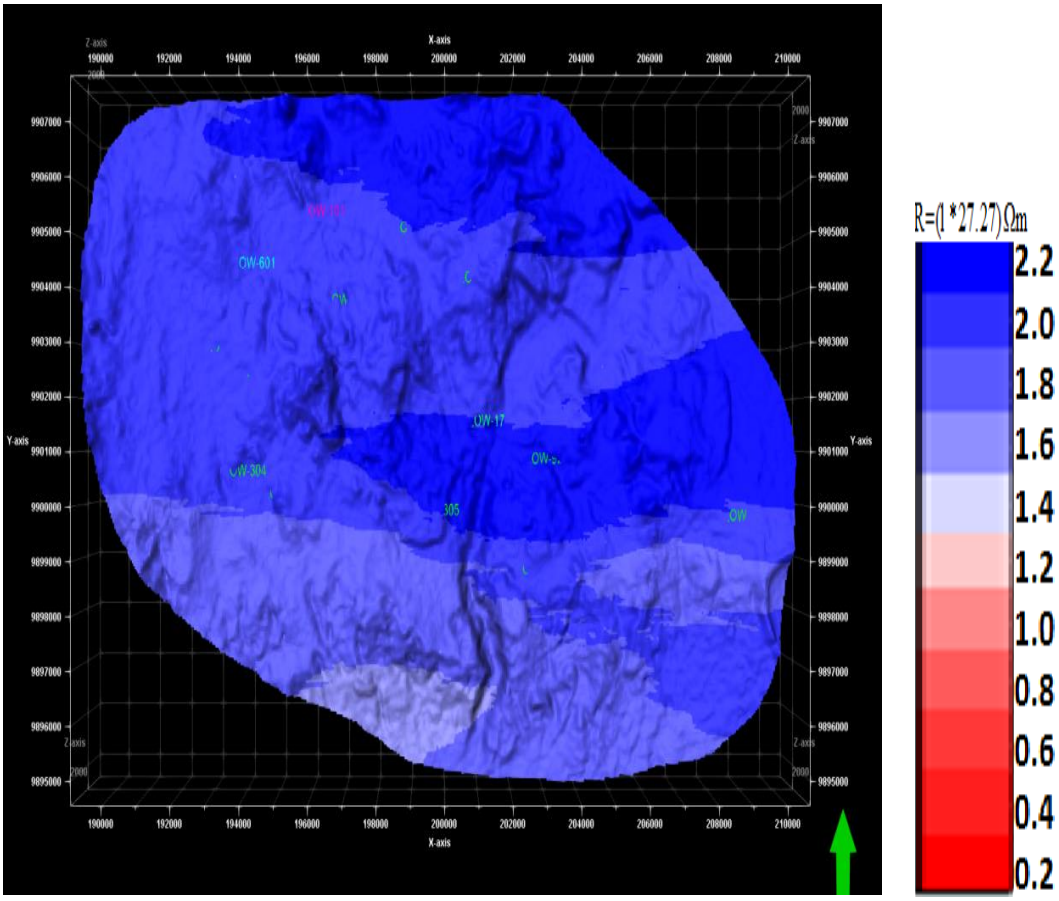

Figure 4.6: Iso-Resistivity map at 2000 m.a.s.l. (close to the surface)

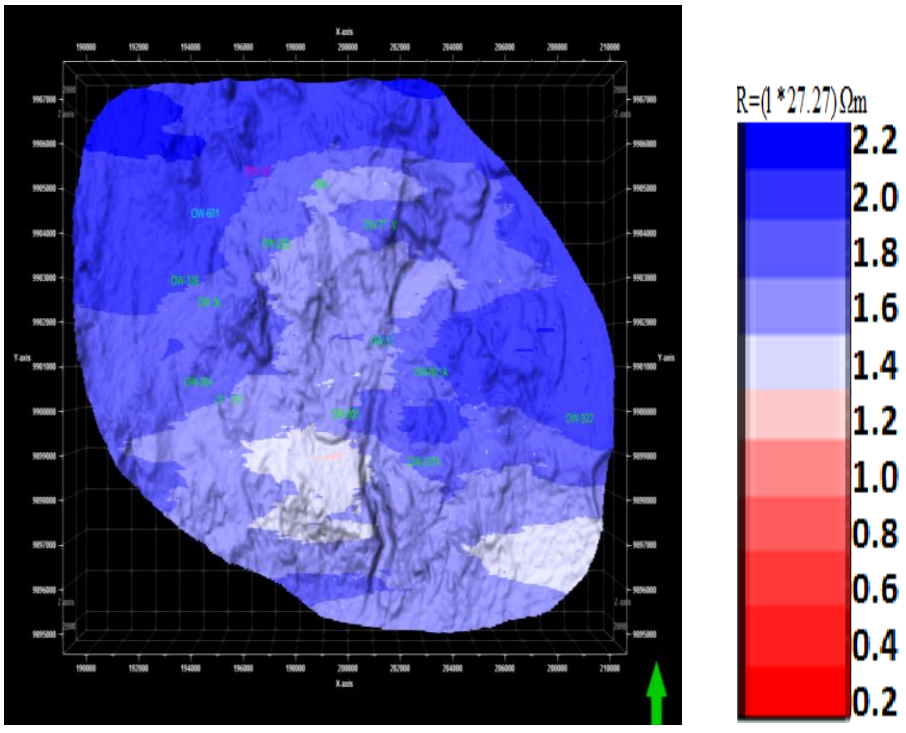

Figure 4.7: Iso-Resistivity map at 1900 m.a.s.l

Resistivity map at 1900 m.a.s.l. presented in Figures 4.7, 4.8 and 4.9(shown in different orientations) show a resistivity of < 15 Ohm-m with the western side of the area covered by conductive formation of resistivity < 10 Ohm-m and the eastern side covered by fairly uniform resistivity of about 10 Ωm covering almost the entire area interpreted to be low temperature alteration minerals like smectite and zeolite formed as a result of hydrothermal alteration fluid filled fractured rock.

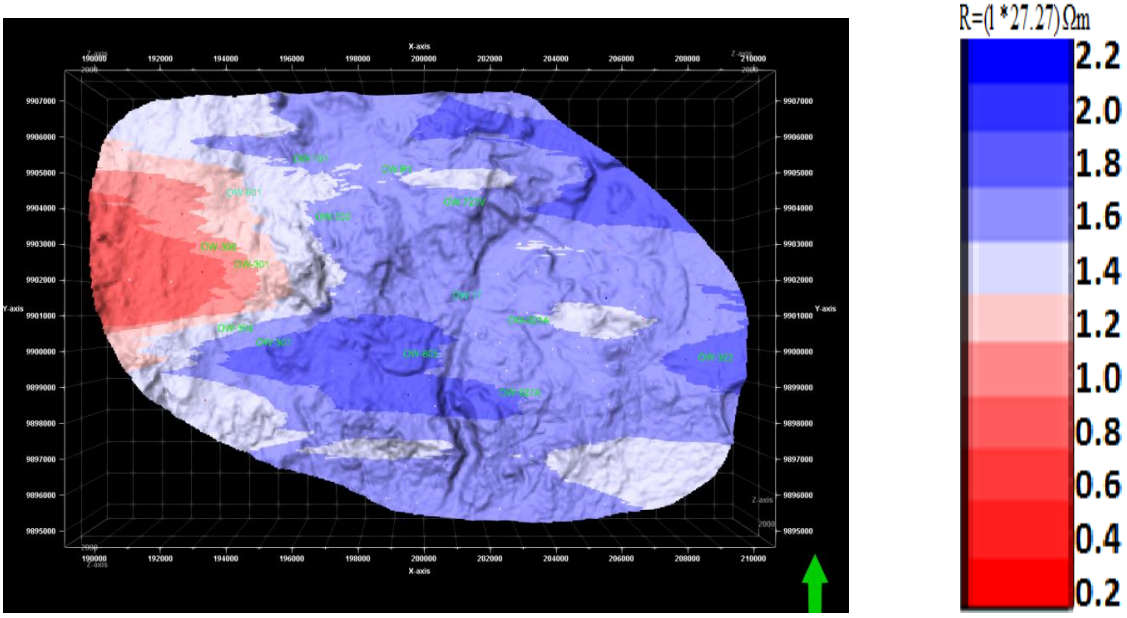

Figure 4.8: Iso-Resistivity map at 1900 m.a.s.l.

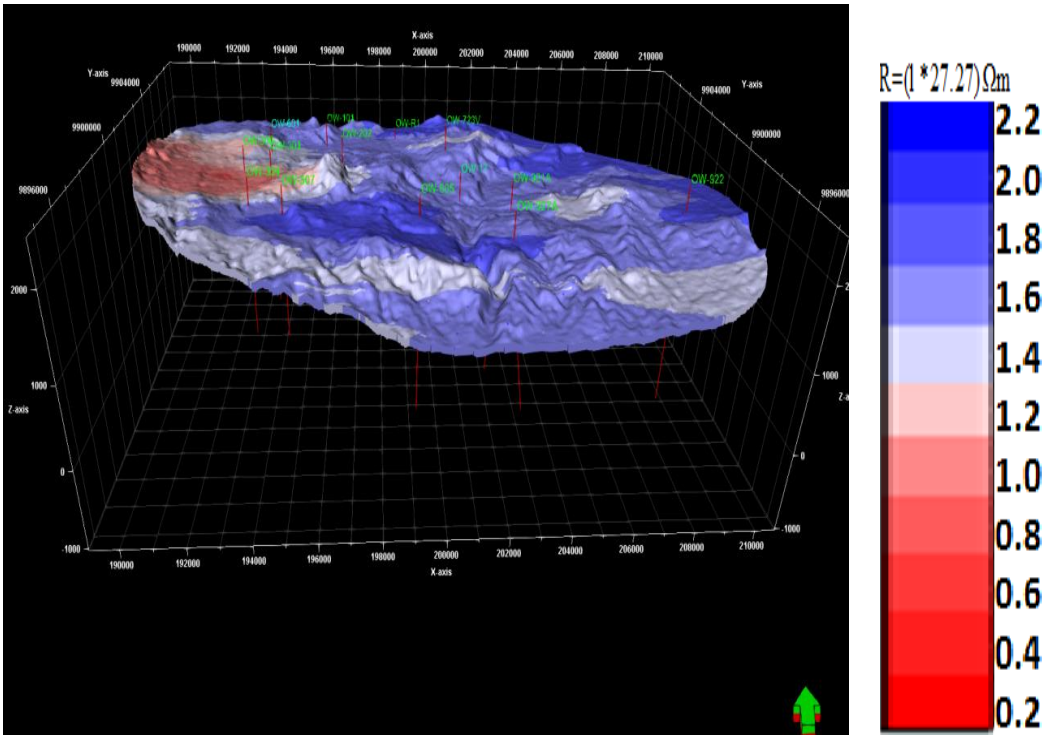

Figure 4.9: Iso-Resistivity map at 1900 m.a.s.l.

Resistivity map at 1000 m.a.s.l. (Figure 4.10 and 11) about 1200m below the ground level shows moderately high resistivity (30 – 60Ωm) to the eastern side of study area and persistent low resistivity of < 10Ωm to the Western side (Oserian). The moderately high resistivity can be attributed to the presence of high temperature secondary minerals such as epidote, chlorite and biotite. The persistent conductive layer to the western side (Oserian) is interpreted to be due to the presence of low temperature alteration minerals like Smectite and Zeolite.

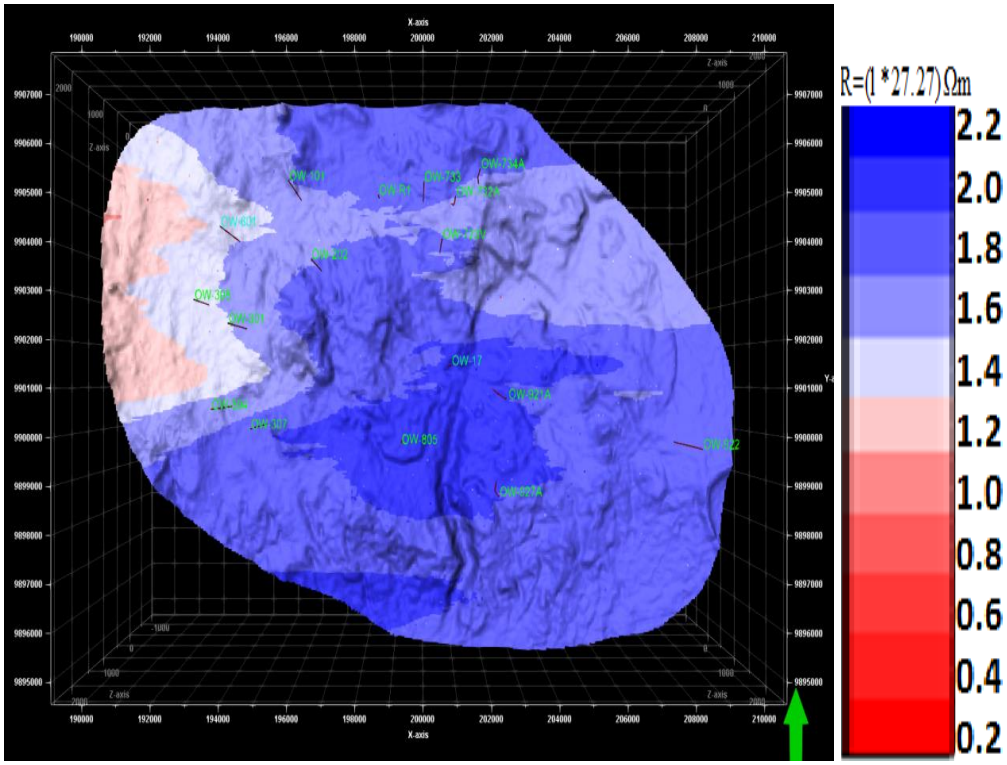

Figure 4.10 : Iso-resistivity map at 1000 m.a.s.l.

Resistivity map at 500 m.a.s.l (Figure 4.12 and 4.13 shown on different orientations) are from about 2000 m below the ground level. The area is covered by medium to high resistivity (30 – 60Ωm). The high resistivity is seen to cover the central part extending to south and eastern side while the medium resistivity is seen to cover the western side (Oserian). The high resistivity is interpreted to be due to the presence of high temperature alteration minerals while medium resistivity is attributed to the presence of low temperature alteration minerals. Findings from the data presented clearly define the resistive feature identified and marked at the center extending southwards may indicate the doming heat source alSso referred to as geothermal upwelling at shallow depth.

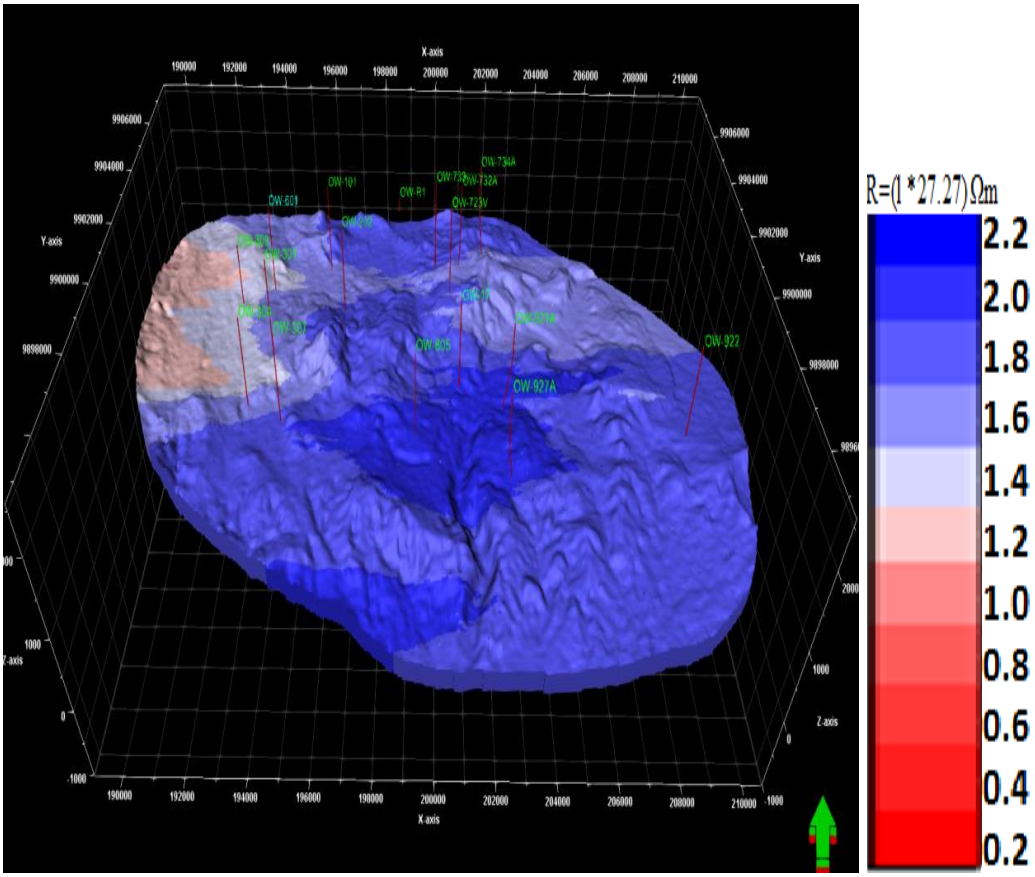

Figure 4.11: Iso-resistivity map at 1000 m.a.s.l.

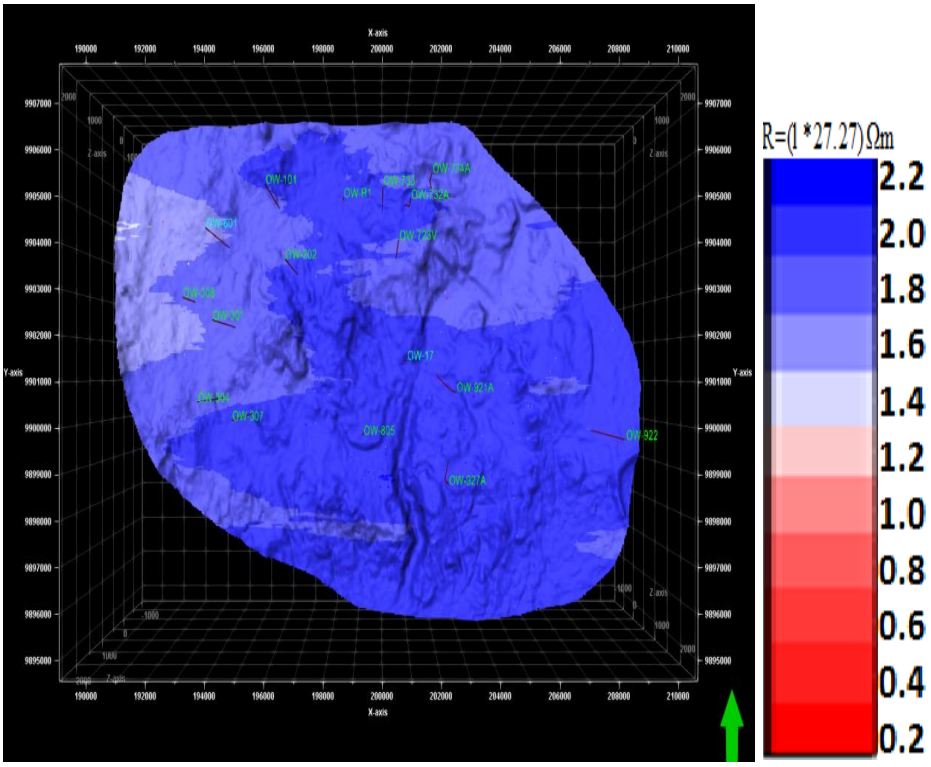

Figure 4.12: Iso-resistivity map at 500 m.a.s.l.

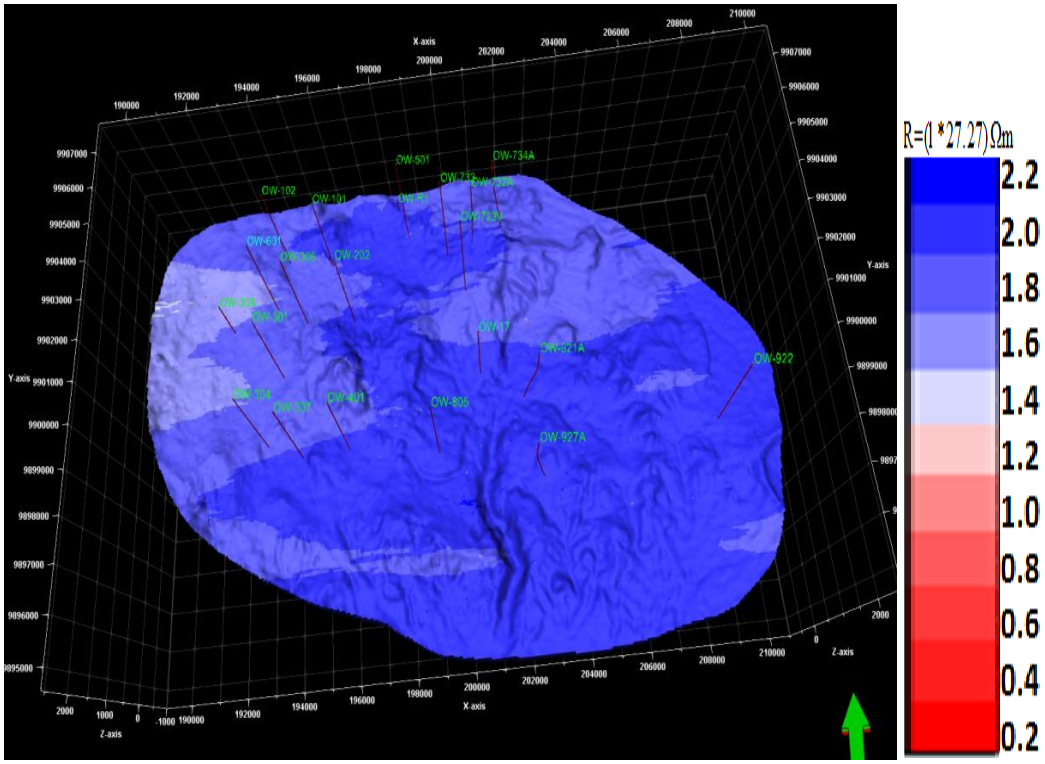

Figure 4.13: Iso-resistivity map at 500 m.a.s.l

Resistivity map at 0 m and 200m.b.s. l (Figure 4.14 and 4.15), the area is covered by medium to high resistivity (30 – 60Ωm). The high resistivity is seen to cover almost the entire area except western side. The high resistivity is interpreted to be due to the presence of high temperature alteration minerals while medium resistivity is attributed to the presence of low temperature alteration minerals. The increased geophysical survey to the east has revealed more information of the presence of high temperature alteration which can be observed at 0 m.

Resistivity map at 2000 m.b.s.l (Figure 4.16), i.e., about 4200 m below the ground level, has a high resistivity starting to diminish and being replaced by low resistivity. The appearing low resistivity anomaly can be associated with the heat source which is structurally controlled.

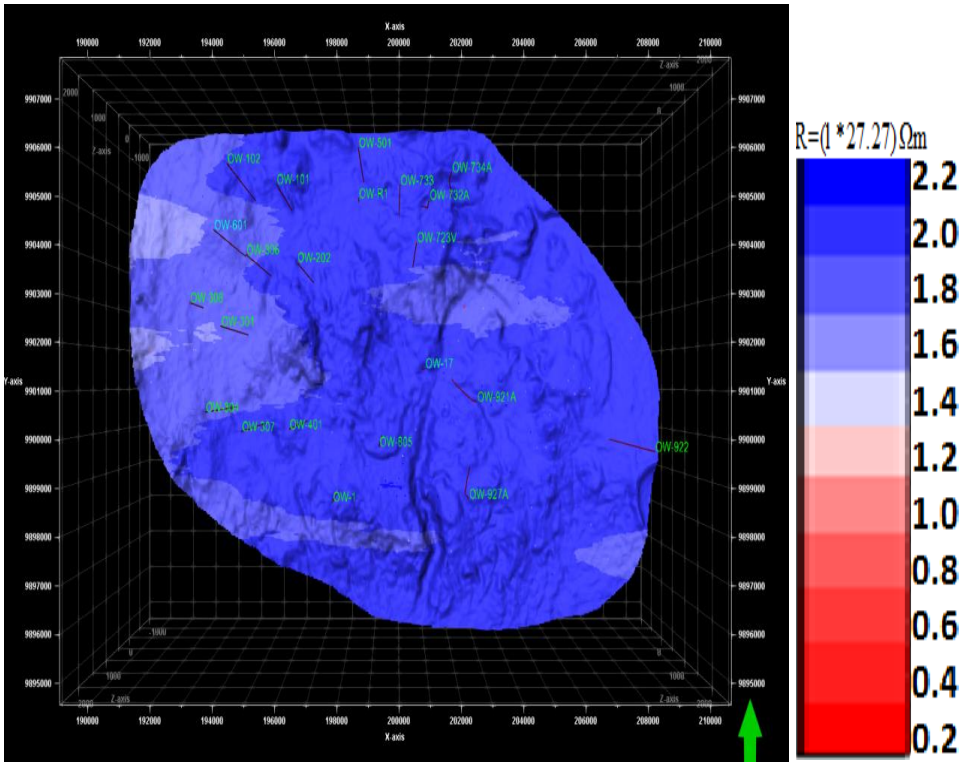

Figure 4.14: Iso-resistivity map at 0 m.

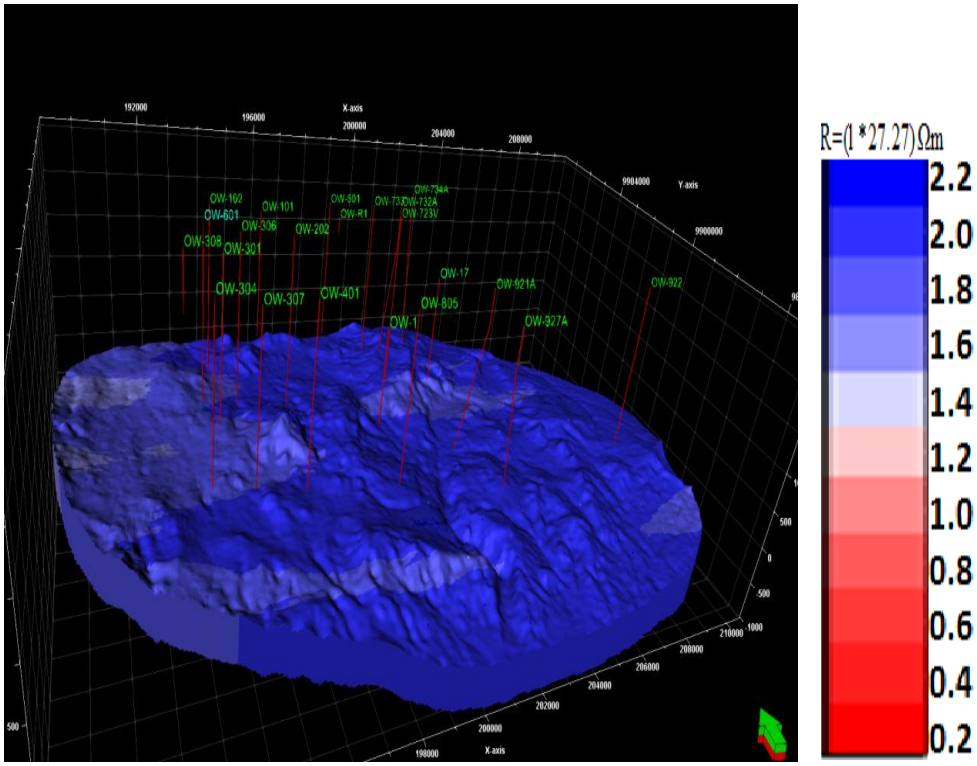

Figure 4.15: Iso-resistivity map at 200m.b.s. l

4.5 Discussion of 1D Inversions

Resistivity structure in most high-temperature geothermal systems is characterized by a low resistivity cap at the outer margins of the reservoir, underlain by a more resistive core towards the inner part. This structure has been found in both freshwater systems as well as brine systems, with the later having lower resistivities values. Comparison of this resistivity structure with data from wells has been carried in high temperature geothermal fields in Iceland and in the East African rift. The results have shown a good correlation with alteration mineralogy. This observation is of great importance, because the temperature dependence of the alteration mineralogy makes it possible to interpret the resistivity layering in terms of temperature, provided that the temperature is in equilibrium with the dominant alteration minerals.

Magnetotelluric (MT) method targets deep hot rocks that act as the heat source for a geothermal system under survey. From the results of the joint inversion of MT and TEM data of the Northwest Olkaria field a fairly good correlation with the available geological information is noted and the following resistivity structure can be deduced as seen on cross-sections and iso-resistivity maps. These areas can be termed as potential reservoirs (Figure 4.16 and 4.17).

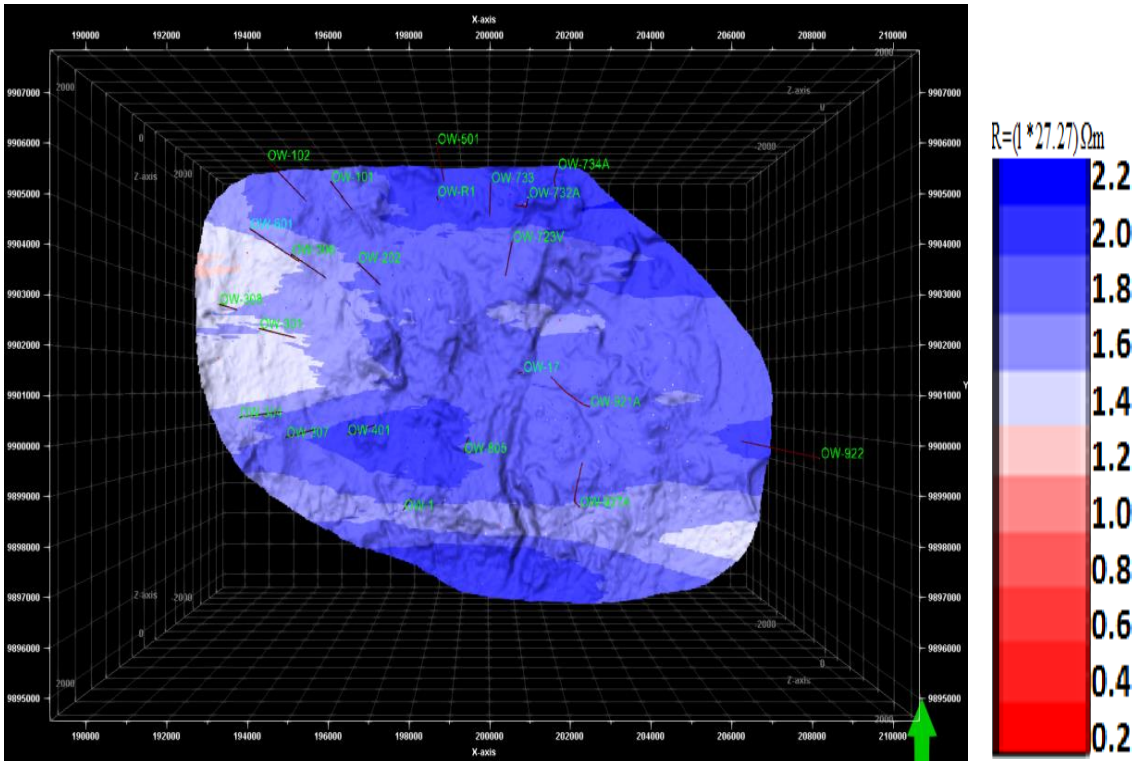

Figure 4.16: Iso-resistivity map at 2000 m.b.s.l

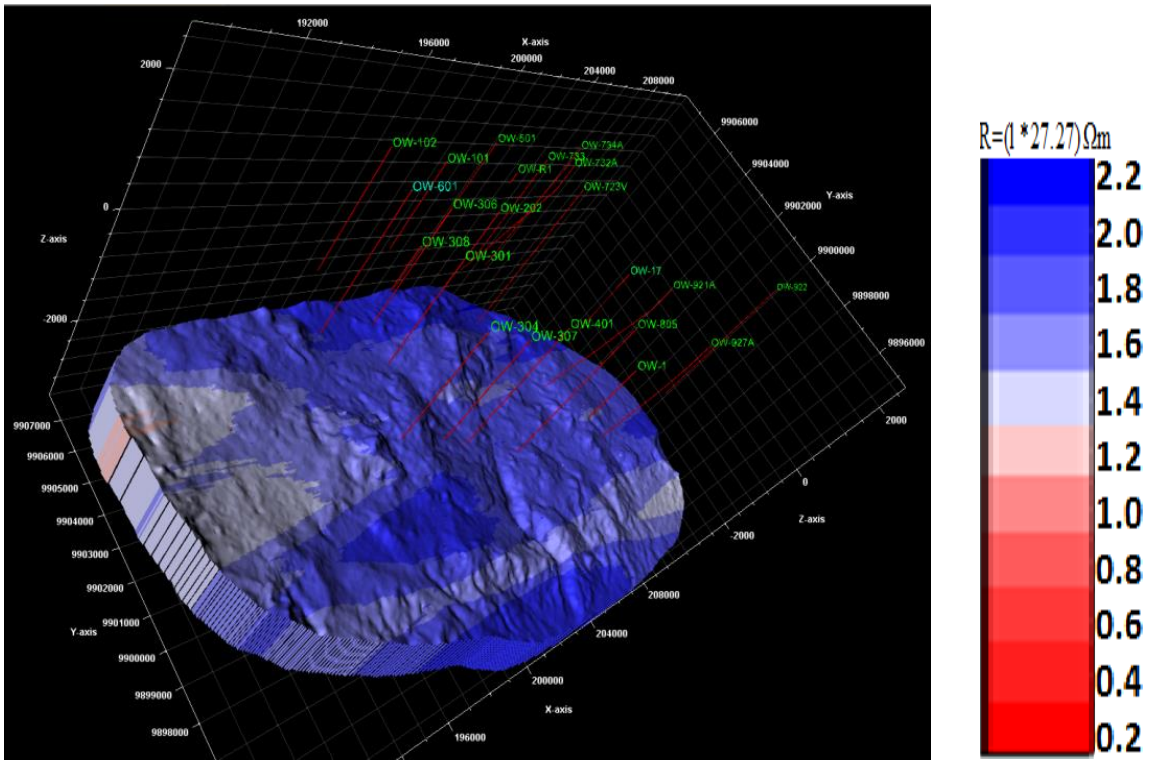

Figure 4.17: Iso-resistivity map at 2000 m.b.s.l

The 1D joint inversion results (Figure 4.16 and Figure 4.17) of Olkaria geothermal complex reveal a resistivity structure with four layered resistivity zones. A shallow superficial high resistivity zone (> 30Ωm) interpreted to be due to unaltered rock formations and the thick pyroclastic cover is observed across the field. This is succeeded by a thick dome shaped conductive layer (< 6Ωm) that extends to about 1900 m.a.s.l in the North West field and thins towards the Central field becoming almost uniform in the South East and the rest of the field. This layer is presumed to be dominated by low temperature alteration minerals such as smectite and zeolite and defines the clay cap. Beneath the base of this conductor is a resistive layer (>15-50) Ωm which is interpreted to be associated with the high temperature secondary minerals such as epidote, chlorite and biotite present in the reservoir. Underlying the resistive layer is another high conductivity layer extending to about 6,000 m.b.s.l (Figure 18) which could be associated with the heat source.

The shallow structure reflects the lithological response of shallow formations, which are quite conductive interpreted to due to the presence of low temperature alteration minerals. It is clear that the low resistivity cap on the western side is different with the low resistivity on the Eastern side. The western side is too conductive and thicker than the eastern side. The alteration mineralogy on the Eastern part of the study area is in agreement with resistivity.

Findings from the data presented clearly define the resistive feature identified and marked at the centre extending southwards may indicate the doming heat source also referred to as geothermal upwelling at shallow depth expressed in the iso-map (Figure 4.18). The appearing low resistivity anomaly is associated with the heat source and geothermal reservoirs which are structurally controlled.

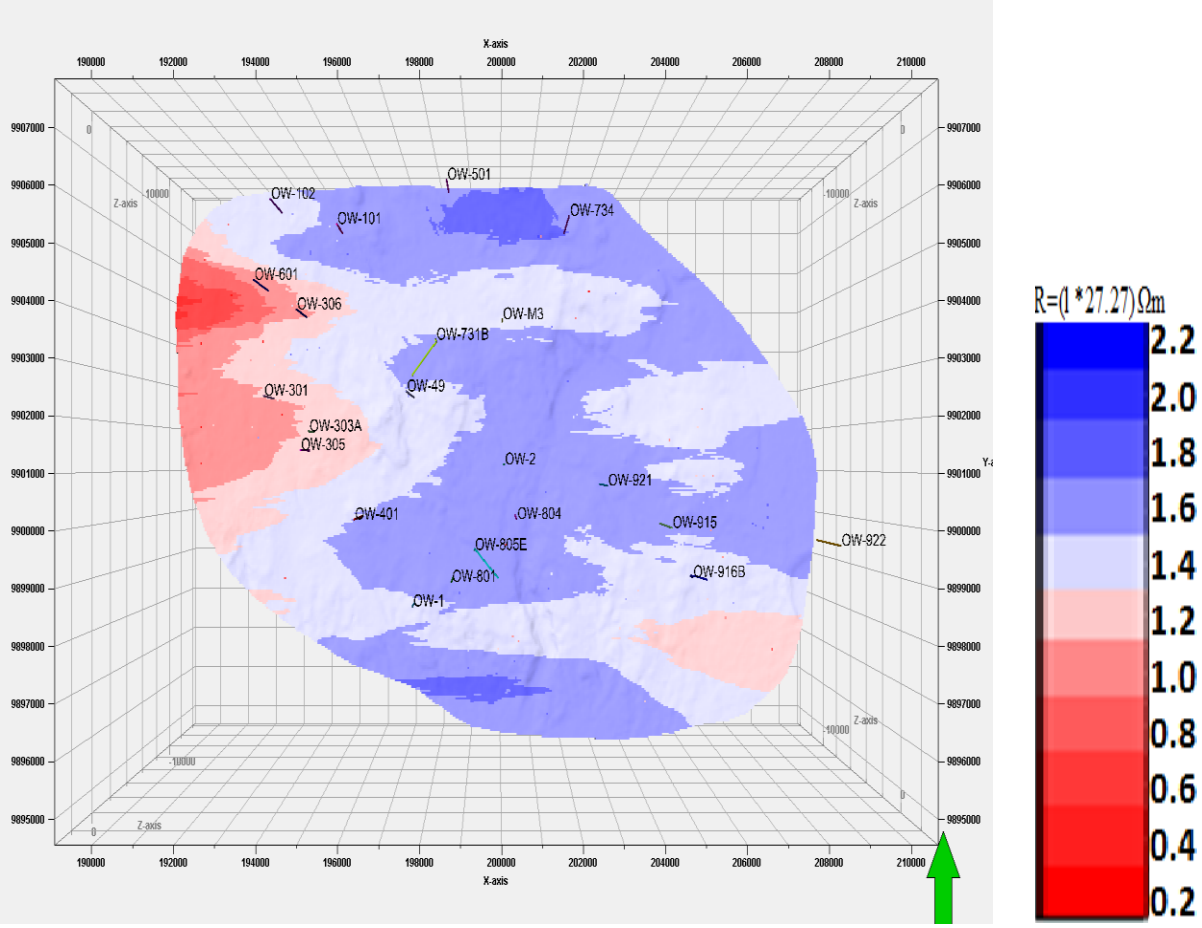

Figure 4.18: Iso-Resistivity maps at 6000 m.b.s.l

CHAPTER FIVE
CONCLUSIONS AND RECOMMENDATIONS

5.1 Conclusions

In this study, modern MT exploration methodology has been applied to structural imaging in the NW Olkaria field. The results have shown that using of MT methodology, useful structural information can be obtained. Like any geophysical method, MT requires a contrast in material properties to image structures.

5.1.1 ID Joint Inversion of Magnetotelluric and Transient Electromagnetic Data

The 1D joint inversion results of NW Olkaria geothermal complex reveal a resistivity structure with four layered resistivity zones:

i. A shallow superficial high resistivity zone (> 30Ωm) interpreted to be due to unaltered rock formations and the thick pyroclastic cover observed across the field.
ii. Thick dome shaped conductive layer (< 6Ωm), that extends to about 1900 m.a.s.l in the North West field and thins towards the Central field becoming almost uniform in the South East and the rest of the field. Dominated by low temperature alteration minerals such as smectite and zeolite and defines the clay cap.
iii. Resistive layer (>15-50) Ωm associated with the high temperature secondary minerals such as epidote, chlorite and biotite present in the reservoir.
iv. High conductivity layer extending to about 6,000 m.b.s.l which could be associated with the heat source.

5.1.2 1D Iso-resistivity maps of Northwest Olkaria field

The iso-maps reveals that:

i. The Illitic clay cap exists between 1900m.a.s.l and 1000m.a.s.l and has a width of 0.9Km.
ii. The reservoir exists between 1000m.a.s.l and 2000m.b.s.l and has a width of 3Km.
iii. The heat source exists at 6000m.b.s.l approximately 8Km from the earth surface at 2000m.a.s.l.
iv. There esists a resource boundary at 500 m.a.s.l.
v. The main reservoir to the western side appears to be deeper than the eastern field.

5.1.3 Intepretation of 1D Magnetotelluric Model of the Northwest Olkaria Field

i. It reveals a high resistive layer of >30 ohm-m that is distributed throughout the region, interpreted as unaltered formation and the superficial deposit on the surface.
ii. Beneath this thin high resistivity layer is a thick layer of a very conductive ≤6 ohm-m dome-like layer that extends up to 1000 m.a.s.l, interpreted as the clay cap
iii. Beneath the base of this conductor is a resistive layer >15-50 ohm-m interpreted as a geothermal reservoir.
iv. Beneath the resistive layer is another high conductivity layer extending to about 6,000 m.b.s.l and it is associated with the heat source.
v. The North West Olkaria prospect has a geothermal potential that exists to the western side of the prospect.

5.2 Recommendations

From the results discussed in this report;

i. It is clear that there exists a potential site for a geothermal resource in the western side. The site has a heat source, a reservoir and a recharge sytem.
ii. The main reservoir to the western side appears to be deeper than the eastern field, therefore it is recommended that the outlet wells should be to the west and the reinjection wells to the east.
iii. Resistivity results from North West indicate a resource boundary to the west at 1000m.a.s.l. therefore further drilling and design can be well guided by the model.

In terms of future work, the following recommendation should be the focus of future research: Other geophysical methods such as seismic and gravity be deployed in the area to complement this study.

REFERENCES

Abdelfettah, Y., Tiercelin, J. J., Tarits, P., Hautot, S., Maia, M., and Thuo, P. (2016). Subsurface structure and stratigraphy of the northwest end of the Turkana Basin, Northern Kenya Rift, as revealed by magnetotellurics and gravity joint inversion. *Journal of African Earth Sciences*, 119, 120-138.

Africa, J. R. (2013). 1D Inversion of MT and TEM data with application of sounding from Krýsuvík, SW-Iceland and a review of MT/TEM data from Bacman geothermal project, central Philippines. *UNU-GTP, Iceland*, report number 5, 22 pp.

Alexander, R. (2013). The project pipeline for global geothermal project s. *The Status of Global Geothermal Power Development,* 25, 56pp.

Árnason, K. (2006). TEMTD, a programme for 1-D inversion of central-loop TEM and MT data. Short manual. *Iceland GeoSurvey - ISOR,* internal report, 17 pp.

Awea, H. (2015). Wind Energy Facts at a Glance, *U.S. Wind Energy Capacity Statistics,* 50, 59-61.

Bedrosian, P. A., Unsworth, M.J., and Wang, F. (2001). Structure of the AltynTagh Fault and Daxue Shan from magnetotelluric surveys: Implications for faulting associated with the rise of the Tibetan Plateau, *Tectonics* (20), 4, 474-486.

Berdichevsky, M., and Dmitriev, V. (2002). Magnetotelluric in the context of the theory of ill posed problems: 12.2 Magnetotelluric in exploration for oil and gas, edited by Keller, G.V., published by *Society of Exploration Geophysicists*.36, 65-72.

Bertani, R. (2005). World geothermal power generation in the period 2001–2005, *Geothermics*, 34, 651–90.

Boashash, B. (2015). Time-frequency signal analysis and processing: a comprehensive reference. *Academic Press* 65, 23-45.

Cagniard, L. (1953). Basic theory of the Magnetotelluric method, *Geophysics*, 18(3), 605-635

Cantwell, T., and Madden, T.R., (1960). Preliminary report on crustal Magnetotelluric measurements, *J. Geophys.Res.*, (65), 12, 4202-4205.

Christiansen, A. V., Auken, E., and Sørensen, K. (2006). The transient electromagnetic method. *Groundwater geophysics*, 56, 642-647

Christopherson, K. R. (1991). Applications of Magnetotellurics to petroleum exploration in Papua New Guinea: A model for frontier areas, *The Leading Edge of Exploration*, 65, 39-45.

Christopherson, K. R. (2002). EM in the 21st Century-Looking for oil, gas and water, 16th Workshop on Electromagnetic Induction in the Earth, *Santa Fe* 16, 63-98.

Dakhnov, V. N. (1962). Geophysical well logging, *Colorado School of Mines*, 57(2), 445-449

DeGroot-Hedlin, C., and Constable, S.C. (1990). Occam's Inversion to generate smooth, two-dimensional models from Magnetotelluric data, *Geophysics*, 55, 1613-1624.

DeGroot-Hedlin, C. (1991). Short Note: Removal of Static shift in tow dimensions by regularized inversion, *Geophysics*, 56, 2102-2136.

Durham, R. L. (2017). Potential field modeling across the neodymium line defining the paleoproterozoic-mesoproterozoic boundary of the south-eastern margin *Laurentia*.36, 54-56.

El Bassam, N. (2012). Options of Renewable Energy Technologies in Restructuring the Future Energy Generation and Supply in Regional and Global Context, *International Research Centre for Renewable Energy, 4, 31-27.*

Flóvenz Ó.G., Hersir G.P., Sæmundsson K., Ármannsson H. and Friðriksson Þ. (2012). Geothermal Energy Exploration Techniques. Sayigh A, (ed.), *Comprehensive Renewable Energy*, 7, 17-24.

Fox, L. (2003. Past, Present and Future of Magnetotellurics, Presentation *to the KEGS 50th Anniversary Conference, Toronto, Canada,* 23,45-47.

Gamble, T. D., Goubau, W. M., and Clark, J. (1979). Magnetotelluric with a remote magnetic reference, *Geophysics*, 44, 53-68.

Ghilardi, A. (2016), Spatiotemporal Modelling of Fuel Wood Environmental Impacts: Towards Improved Accounting for Non-renewable Biomass. *Environmental Modeling & Software*, 82, 241-254.

Girdler, R. W. (ed.). (2013). East African Rifts. Elsevier. (gravity and magnetic),40,52-68

Gritsevskyi, A. (2017). Renewable vs. non-renewable energy sources, forms and technologies, *IAEA*, 5, 12pp.

Groom R. W., and Bailey, R.C. (1989). Decomposition of Magnetotelluric impedance tensor in the presence of local three-dimensional galvanic distortion, *J. Geophys*. (94), 1913-1925.

Hersir, G. P., and Björnsson, A. (1991). Geophysical exploration for geothermal resources, principles and applications. *UNU-GTP, Iceland*, report 15, 19-21.

Hersir, G. P., and Árnason, K. (2009). Resistivity of rocks. Presented at "Short Course on Surface Exploration for Geothermal Resources", organized by UNU-GTP and LaGeo, in Ahuachapan and Santa Tecla, *El Salvador*, 67(5), 368-371.

Ingerov, O. I., Fox, L., Golyashov, A., and Colin, A. (2009). Non-grounded Surface Electroprospecting Technique. Extended Abstract, *EAGE Conference and Exhibition-Amsterdam, the Netherlands*, 71, 251.

Jones, A. G. (1988). Static shift of magnetotelluric data and its removal in a sedimentary basin environment. *Geophysics*, 53(7), 967-978.

Kanda, I. K., Rankas, L., Bett, E.K., Kipngok, J.K., Mutonga, M., Sosi B., Gichira, J., Mwakirani, R.M., Mboin, I. J., Ndongoli, C., Odundo, L., Ouko, E., Mwawasi, H. (2011). Paka Prospect: Investigations of its geothermal potential. *GDC Internal report* 10, 14pp.

Kenya Gazette. (2009). Gazette notice no.6065, National task force on accelerated.

Kearey, P., Brooks, M., and Hill, I. (2013). An introduction to geophysical exploration. *John Wiley*,6,88 pp.

KenGen. (2004). Menengai Volcano: Investigations for its geothermal potential-a geothermal resource assessment project, *internal report*, 43,12pp.

KenGen Report. (2014). Study of the Greater Olkaria Geothermal Fields, *internal report*, 3,75pp.

Khazri, D., and Gabtni, H. (2018). Geophysical methods integration for deep aquifer reservoir characterization and modelling (SidiBouzid basin, central Tunisia). *Journal of African Earth Sciences*, 138, 289-308.

Kiva, I. N. (2009). GOK responses to the energy crisis. *Presented during the experts' roundtable on the current energy crisis in Kenya*, 67, 38-40.

Lagat, J. K., Omenda, P. O., Mungania, J., Mariita, N. O., Wambugu, J. M, Opondo, K. Ofwona, C., Mwawongo, G., Kubo, B. M., Wetangula, G. (2007). Geo-scientific Evaluation of the Paka Geothermal Prospect, *KenGen Internal report*, 60,7pp.

Ľudovít, C., Kristof, V., Stanislav K. S., Katin, M., Marci, M. (2010). Renewable Energy Sources, *ZelezaRuda-Spicak, University of West Bohemia, Czech Republic*, 5, 65pp.

Marcus, G. (1999). Magnetic distortion of GDS transfer functions: An example from the Penninic Alps of Eastern Switzerland revealing a crustal conductor, *Earth Planets Space*, 51, 1023–1034.

Madden, T. R., and Nelson P. (1964. A defense of Cagniard's magnetotelluric method, in Magnetotelluric Methode, edit by Vozoff, K., *Society of Exploration Geophysicists., Tulsa.*65,96-103.

Mackie, R. L., and Rodi, W. (1996). A nonlinear conjugate gradients algorithm for 2-D magnetotelluric inversion: *American Geophysical Union, San Francisco, Califonia*, 23,123-128.

Mariita, N. O. (2000). An integrated geophysical study of the northern Kenya rift crustal structure: implications for geothermal energy prospecting for Menengai area, *A PhD dissertation, University of Texas at El Paso, USA*, 60-65.

Matsuo K., and Negi, T. (1999). Oil exploration in difficult Minami-Noshiro area- Park Two: Magnetotelluric Survey, *The Leading Edge of Exploration*,6,45-63.

Mechie, J., Keller, G. R., Prodehl, C., Khan, M.A. and Gachiri, S. J. (1997**).** A model for the structure, composition and evolution of the Kenya rift, *Tectonophysics*, 278,95-11.

Mulwa, J., and Mariita, N. (2013). A comparative analysis of gravity and microseismic results from Arus-Bogoria geothermal prospect, Kenya. *Scholarly Journal of Scientific Research and \Essay (SJSRE), ISSN*, 2315-6163.

Mulwa, J. K., and Mariita, N. O. (2015). Dyking processes in Arus-Bogoria geothermal prospect in Kenya revealed using gravity and microseismic data. In *37th New Zealand Geothermal Workshop: The next 10,000 Megawatts*. University of Auckland, New Zealand Geothermal Association, 37, 20-23.

National Energy Policy Act. (1992). The Pacific Northwest Electric Power Planning and Conservation *Act of 1980 12H*, 839a, (16), 84 pp.

Odera, P. A. (2016). Assessment of EGM2008 using GPS/levelling and free-air gravity anomalies over Nairobi County and its environs. *South African Journal of Geomatics*, 5 (1), 17-30.

Ofwona, C. (2008). Geothermal Resource Assesment-Case Example Olkaria 1, Presented at Short Course III on Exploration for Geothermal Resources, *UNU- GTP*, 3, 18-19.

Oldenburg, D. W. (1979). One dimensional inversion of natural source Magnetotelluric observations, *Geophysics*, 44, 1218-1244.

Omenda, P. (1998). Geochemical evidence for syeniticprotholith. *African Journal of Sciences and Technology. Science and Engineering series,* 1,68pp.

Omenda, P. (2000). Anatectic origin for Comendite in Olkaria geothermal field, Kenya Rift; Geochemical evidence for syeniticprotholith. *African Journal of Sciences and Technology. Science and Engineering series,* 1(68), 39-47.

Omenda, P., and Simiyu, S. (2015). Country update report for Kenya 2010–2014. *Proceedings World Geothermal*, 34, pgs 60-72.

Ouma, P. A. (2010). Geothermal exploration and development of the Olkaria geothermal field. Paper presented at *Short Course V on Exploration for Geothermal Resources organized by UNU-GTP, GDC and KenGen, at Lake Bogoria and Lake Naivasha, Kenya*, 5, 16pp.

Parasnis D. S. (1997). Principles of Applied Geophysics. *Chapman and Hall, U. S. A.* 61,103pp.

Park, S. K. Thompsom, S. C., Rybin, A., Batalev, V., and Bielinski, E. (2003). Structural constraints in neotectonic studies of thrust faults from the magnetotelluric method, Kochkor Bain, Kyrgyz Republic, *Tectonics,* (22),2, 1013.

Pellerin, L., and Hohmann, G.W. (1990). Transient electromagnetic inversion: A remedy for magnetotelluric static shifts, *Geophysics*, 55, (9), 1242-1250.

Picha, F. J. (1996). Exploration for hydrocarbon under thrust belts – a challenging new frontier in the Carpathians: *AAPG Bulletin*, (80), 10, 1547-1564.

Prodehl, C., Ritter, J., Mechie, J., Keller, G. R., Khan, M.A., Fuchs, K., Nyambok, I. O., and Obel, J. D. (1997). The KRISP 94 Lithospheric investigation of southern Kenya-the experiments and their main results in Stress and stress release in the Lithosphere, *Tectonophysics*, 278, 121-148.

Renaut, R. W., Owen, R. B., and Ego, J. K. (2017). Geothermal activity and hydrothermal mineral deposits at southern Lake Bogoria, Kenya Rift Valley: Impact of lake level changes. *Journal of African Earth Sciences*, 129, 623-646.

Schumucker, U. (1970). Anomalies of the magnetic variations in the South-Western United States, Bull. Scripps Inst. Oceanogr.13, *University of California Press,* 13, 67-71.

Shako, L., and Wamalwa, A. (2014). GIS Applications in Heat Source Mapping in Menengai Geothermal Field. In *Proceedings of the 5th African Rift Geothermal Conference*, 5, 88-96.

Simiyu, S. M., and Keller, G. R. (1997). Integrated geophysical analysis of the East African Plateau from gravity anomalies and recent seismic studies. *Tectonophysics,* 278, 291-314.

Simiyu, S. M., and Keller G. R. (2001). An integrated geophysical analysis of the upper crust of the southern Kenya rift, *Geophysical journal international*, 147,543-556.

Simpson, F., and Bahr, K. (1956). Practical Magnetotellurics. *Cambridge University Press, Cambridge; New York,* 2005, 69pp.

Smith, J. T., and Booker, J. R. (1991). Rapid inversion of two and three-dimensional magnetotelluric data, *Journal Geophysical. Research.*, 96, 3905-3922.

Sternberg, B. K., Wash, B. J. C., Pullerin, L. (1988). Correction for the static shift in Magnetotellurics using Transient Electromagnetic soundings. *Geophysics,* 53, 1459-1468.

Telford, W. M., Geldart, L. P., and Sheriff, R. E. (1990). Applied geophysics, Cambridge *university press,* 1,110-117.

Tikhonov, A. N. (1950). Determination of the electrical characteristics of the deep state of the earth's crust, Dok. Akad. Nauk, *USSR,* 73(2), 295-297.

Wadge, G., Biggs, J., Lloyd, R., and Kendall, J. M. (2016). Historical volcanism and the state of stress in the East African Rift System. *Frontiers in Earth Science*, 4, 86pg.

Wait, J. R. (1954). On the relation between telluric currents and the Earth's magnetic field, *Geophysics*, 19, 281-289.

Wamalwa, A. M., Kevin, L. M., and Laura, F. S. (2013). Geophysical characterization of the Menengai volcano, central Kenya Rift from the analysis of the magnetotelluric and gravity data, *geophysics*, 78(4), 187-199.

Wamalwa, A. M., and Serpa, L. F. (2013). The investigation of the geothermal potential at the Silali volcano, Northern Kenya Rift, using electromagnetic data. *Geothermic*, *47*, 89-96.

Ward, S. H., and Wannamaker, P. E. (1983). The MT/AMT electromagnetic method in geothermal exploration, *UNU-GTP, Iceland, report* 5, 107 pp.

Watts, M. D., and Pince, A. (1998). Petroleum exploration in overthrust area using magnetotelluric and seismic data, *SEG expanded abstract, New Orleans* 5, 96-106.

Watts, M. D., Alexandros, S., Eleni, K., and Mackie, R. (2002). Magnetotelluric applied to sub-thrust petroleum exploration in Northern Greece, *European Commission Research Directorate-General Report,* 9, 85-102.

West-JEC. (2006). The Olkaria Optimization Study – Phase I final report. *West Japan Engineering Consultants,* 1, 52-59.

Wu, F. T. (1968). The inverse problem of Magnetotelluric sounding, *Geophysics*, 33(6), 972-979.

Vozoff, K. (1991). The Magnetotelluric method, in Electromagnetic methods in Applied Geophysics: M. N. Nabighian, Ed., *Society of Exploration Geophysicists, Tulsa, Oklahoma,* 2(B), 641-711.